

THE INTERNAL STRUCTURE OF MODEL AND NATURAL SALT DOMES

Experimental Modeling of Salt Diapirs: Final Report

by

**M. P. A. Jackson
Bureau of Economic Geology
The University of Texas at Austin
Austin, Texas**

and

**Christopher J. Talbot
Institute of Geology
University of Uppsala
Uppsala, Sweden**

Assisted by Reinold Cornelius and Ronald Arvidsson

**Prepared for the U.S. Department of Energy Office of Nuclear Waste Isolation under Contract No.
DE-AC97-83WM46651**

**Bureau of Economic Geology
W. L. Fisher, Director
The University of Texas at Austin
University Station, Box X
Austin, Texas 78713**

March 1985

TABLE OF CONTENTS

ABSTRACT	1
INTRODUCTION	1
EXPERIMENTAL DESIGN AND GOALS	2
EXPERIMENTAL PROCEDURE	2
APPLICATION OF EXPERIMENTS TO MAIN FIELDS OF STUDY	4
Internal Structures	4
Downbuilding Versus Upbuilding	5
Differential Loading, Including Prograding Cover	5
First-Order Movement Cells	6
SCOPE OF THIS REPORT	7
FACTORS CONTROLLING THE GROWTH OF MUSHROOM-SHAPED DIAPIRS	7
EXPERIMENTAL RESULTS	11
GENERAL ANATOMY OF MUSHROOM STRUCTURES	11
SPECIFIC ANATOMY OF MODEL MUSHROOM DIAPIRS	17
Threefold Diapirs	18
Fivefold Diapirs	18
Sevenfold Double Diapirs	18
Vortex Structures	23
MUSHROOM DIAPIRS IN NATURE	27
Canadian Arctic Islands	29
Northwest German Plain	29
U.S. Gulf Coast	32
SOME IMPLICATIONS TO NUCLEAR WASTE ISOLATION	34
ACKNOWLEDGMENTS	40
REFERENCES	41
APPENDIX 1: Summary of Experiments Carried out in March and April 1984, at the Hans Ramberg Tectonic Laboratory, Uppsala, Sweden	44
APPENDIX 2: Experimental Procedure	48
APPENDIX 3: Analytical Procedure	56

Figures

1. The processes of diapir upbuilding and downbuilding compared	3
2. Formation of diapir caps	8
3. Schematic summary of the effects of viscosity contrast on shapes of immature and mature domes based on experimental and mathematical modeling by other researchers	10
4. Starting configuration of five models before acceleration in the centrifuge.	12
5. Block diagrams in isometric projection showing the number of domes produced in two similar experiments.	13
6. Schematic symmetric fivefold mushroom diapir in vertical section showing terminology of major folds	15
7. Block diagrams of schematic fivefold diapirs to show relation between vertical section and horizontal section	16
8. A variety of model domes in vertical section	19
9. Vertical and horizontal sections through threefold asymmetric model diapirs	21
10. Vertical and horizontal sections through a fivefold asymmetric model diapir	22
11. A sevenfold double-stalk diapir formed by lateral fusion of the caps of two coeval model diapirs	24
12. Vertical and horizontal sections through a sevenfold asymmetric double diapir with a draped-arm structure shown schematically	25
13. Vertical and horizontal sections through a schematic fivefold asymmetric diapir with vortex structure	26
14. Vertical sections through two model diapirs at different stages of development	28
15. Barrow Dome, an exposed composite diapir of gypsified anhydrite-mafic plutonite in the Sverdrup Basin, Arctic Canada	30
16. Cross section of Asse Dome, West Germany	31
17. Map and three cross sections of Gorleben Dome, West Germany	33
18. Palangana Dome, South Texas	35
19. Horizontal section through northwest sector of Belle Isle Dome, Louisiana, at the mined 354-m level	36
20. The effect of salt dome shape (vertical sections) on the integrity of a repository	38
21. Internal and external mushroom structure	39

ABSTRACT

To improve our understanding of the internal structure of salt stocks, we conducted 30 centrifuge experiments that produced hundreds of model diapirs under artificial acceleration generally equivalent to 1,200 times that of normal gravity. Most of these experiments were geometrically and dynamically scaled to be equivalent to U.S. Gulf Coast salt domes. The domes were modeled under static overburdens and, for the first time, under aggrading and prograding overburdens. This report concentrates on the internal structure of mushroom-shaped domes, which theoretically exist in nature and are demonstrated in natural examples in the U.S. Gulf Coast, Canada, and West Germany. The experimental results enable the extremely complex internal structure of mushroom-shaped salt domes to be recognized and understood. This recognition is vital because a mushroom structure would threaten the integrity of a hypothetical repository by creating a plumbing system composed of country rocks infolded from below the diapir cap and extending to near the dome center.

INTRODUCTION

Salt diapirs are one of several types of rock body being considered by the Salt Repository Project Office program as geologic hosts for storage of high-level nuclear waste. However, structural geologists currently understand little of the internal structure of salt stocks. The structural geology of salt domes contributes to important practical aspects such as rock mechanics and fabrics, in-situ stresses, mapping inclusions of potentially leaky country rock, and prediction of diapir shape at depth. The present study aims at improved understanding of the internal structures and external shapes of salt domes in general as a guide to the detailed exploration of any salt dome selected as a repository for nuclear waste.

The study began in January 1984 and is built around eight weeks (from March 5 through April 27, 1984) of intensive experimental modeling at the Hans Ramberg Tectonic Laboratory at the University of Uppsala, Sweden. Out of 33 experiments run, 30 were carried out in a centrifuge under artificial acceleration generally equivalent to 1,200 times that of normal gravity. Most model diapirs, which developed in layered mixtures of silicone putty and

modeling clay, were dynamically scaled to resemble their natural analogs in the U.S. Gulf Coast.

EXPERIMENTAL DESIGN AND GOALS

At Uppsala priority was given to designing and carrying out as many centrifuge experiments as possible, rather than spending days analyzing the results of each experiment before proceeding with the next one. The experiments were designed to elucidate four aspects:

1. Internal structure revealed by passive (mechanically inactive) marker layers, which provide qualitative information on the finite strain within the diapirs during their flow and emplacement.
2. Effects of downbuilding (syndepositional diapir growth beneath aggrading cover) versus upbuilding (postdepositional diapir growth beneath static cover) (fig. 1).
3. Differential loading, especially by prograding cover.
4. Large-scale movement cells, comprising the entire diapiric system of buoyant source layer and heavy cover, and the relation between diapiric jets and walls.

EXPERIMENTAL PROCEDURE

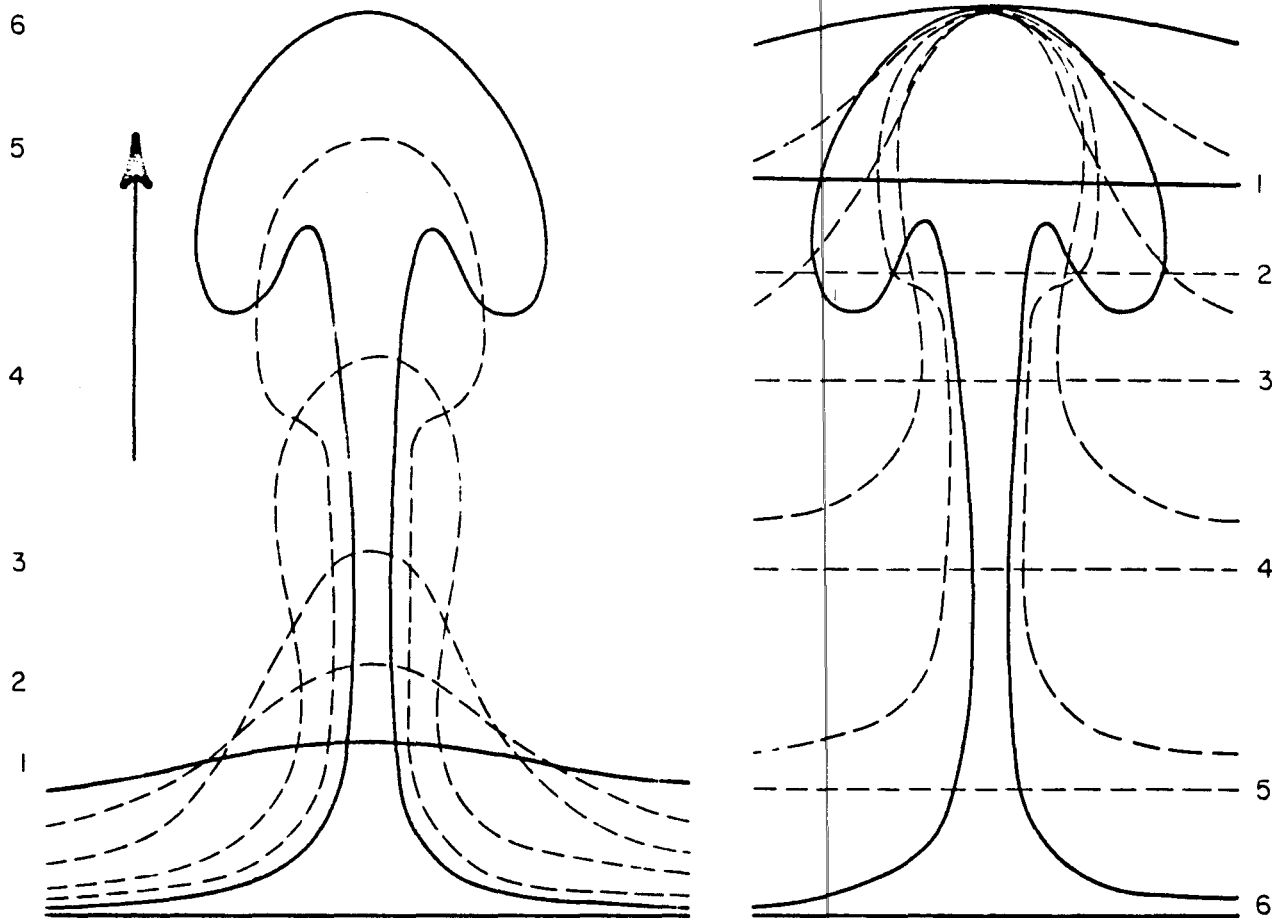
All the experiments are summarized in appendix 1. Appendix 2 describes the experimental procedure: materials used, material preparation, testing procedure for material properties, model design, model construction, model acceleration, model dissection, and documentation. Appendix 3 describes data handling and data analysis and synthesis procedures.

The experiments constitute four different groups, based on the experimental conditions imposed during the growth of the model structures. "Source layer" refers to the model salt and "cover" refers to the model sedimentary overburden.

(1) In the aggrading group of diapirs, cover was added as tabular layers, each of which was commonly different from those immediately above or below but which had uniform thickness and mechanical properties. In the upbuilding models, the entire thickness of cover

TWO EXTREMES OF GROWTH

surface



UPBUILDING

Postdepositional
Rising crest
Static base

DOWNBUILDING

Syn depositional
Static crest
Sinking base

GA2892

Figure 1. The processes of diapir upbuilding and downbuilding compared. Diapir shape at different growth stages based on finite-element modeling by Berner and others (1972).

was added before the first acceleration in the centrifuge; the diapirs grew postdepositionally from depth to near the surface (fig. 1). In the downbuilding models, increments of cover were added before each of several periods of acceleration; the diapirs grew syndepositionally, remaining near the surface of the model throughout growth. Downbuilding had not previously been modeled by the centrifuge technique.

(2) In the prograding group of diapirs, cover was added--usually in many increments--as nontabular layers of nonuniform thickness; the diapirs grew syndepositionally under the influence of differential loading. Progradation had not previously been modeled by the centrifuge technique.

(3) In the mercury-cover experiments, a source of silicone putty was overlain by a much thinner layer of mercury to simulate the effect of a thin cover during the early stages of downbuilding. The extreme density inversion allowed larger-than-normal diapiric systems to overturn completely in an hour or two outside the centrifuge under normal gravity during continual observation.

(4) In the piedmont glacier experiments, a source layer was allowed to run down a model valley before spreading out in a piedmont fan over a model plain. The largely two-dimensional structures produced provide some analogies to vertical cross sections through mature salt diapirs, with the advantage that the continual evolution of the internal structures can be observed without sectioning the model.

APPLICATION OF EXPERIMENTS TO MAIN FIELDS OF STUDY

Appendix 1 lists the application of each experiment to one or more of the four groups of experimental goals listed in the previous section.

1. Internal Structures

All diapirs containing internal layers provide information on the finite strain within them during their flow and emplacement. Qualitative inferences on the accompanying stresses can be drawn from the strain pattern. Mushroom-shaped diapirs--those with peripheral hanging

lobes encircling upward infolds--were common in most experiments. Because there are good reasons to expect them in nature (see "Factors controlling the growth of mushroom-shaped diapirs" and "Mushroom diapirs in nature") and because of their important implications to the safety of a salt-dome repository (see "Some implications to nuclear waste isolation"), these structures were given the highest priority of study. Follow-up work will be directed, in part, to deducing qualitatively the orientation of principal stresses during diapir growth.

2. Downbuilding Versus Upbuilding

The process of downbuilding must be common in nature because most of the Gulf Coast diapirs show evidence of syndepositional growth; diapir growth must be by downbuilding if growth is syndepositional. Yet before the 1984 experiments, the process of downbuilding had never been simulated experimentally in the centrifuge.

The following conclusions are based only on casual study during the course of the experiments. The viscosity ratio between cover and source layer (the parameter m) had equal control on the structure of diapirs whether they grow by upbuilding or downbuilding. Differences between domes that grew by upbuilding and domes that grew by downbuilding were smaller than expected: (1) During downbuilding, the initial wavelength expanded as the cover thickened, eventually attaining the same wavelength as upbuilt diapirs; this expansion of wavelength fused some immature diapirs together, forming multistalked diapirs with a single cap. Multiple stalks mean that country rock is present immediately below the center of the cap. (2) Both modes of growth encouraged the formation of salt walls at depth and salt jets near surface after the diapiric system had matured, but during downbuilding these walls are revealed near surface as salt ridges. Further study is required on the shape and style of large-scale movement cells during upbuilding compared with downbuilding.

3. Differential Loading, Including Prograding Cover

Most previous models have simulated diapirism beneath an overburden with laterally uniform properties of thickness, density, viscosity, and so on, which is unrealistic. Some centrifuge models have simulated uneven overburdens, but these have all been static loads. The

most common situation of loading is by prograding sediments. This dynamic process was simulated in the 1984 experiments. All the experiments show the extreme importance of nonuniform cover and boundary conditions on determining the shape, and therefore the internal structure, of diapirs. Prograding deltas and depocenters were successfully simulated; the huge salt nappe defining the Sigsbee Scarp was also modeled. Further study of the models will be directed to the following aspects:

1. The effect of prograding cover on diapir shape and internal strains and stresses
2. The effect of prograding cover on dome spacing
3. The relation between the effects of aggradation and progradation separately and combined
4. First-Order Movement Cells

The first-order movement cell includes the various parts of the diapir itself, its withdrawal basin in the source layer, and all parts of the adjacent cover that show the effects of strain specific to the diapir in the form of thickness changes or deformation structures. An understanding of these movement cells is essential for predicting dome shape at the depths of the diapir stem and root. The 1984 model diapirs pass downward into polygonal walls of "salt," each polygon surrounding a sinking plume (or jet in fluid dynamics terms) of cover. Such polygons appear to link salt diapir roots in offshore Louisiana as well, where good subsurface data have been obtained. They may also be theoretically predictable. Using the experimental models as a basis, we would like to develop a theoretical model to explain why salt jets at surface should link with salt walls at depth (and vice versa for the cover). This model would help answer fundamental questions such as

1. What is the shape of salt stocks at depth?
2. What is the predominant polygon shape, what controls it, and what are the flow patterns of salt?
3. Does a predominance of walls or jets of salt reflect a particular energy level in the movement cell, analogous to the effect of energy levels on the shape of thermal

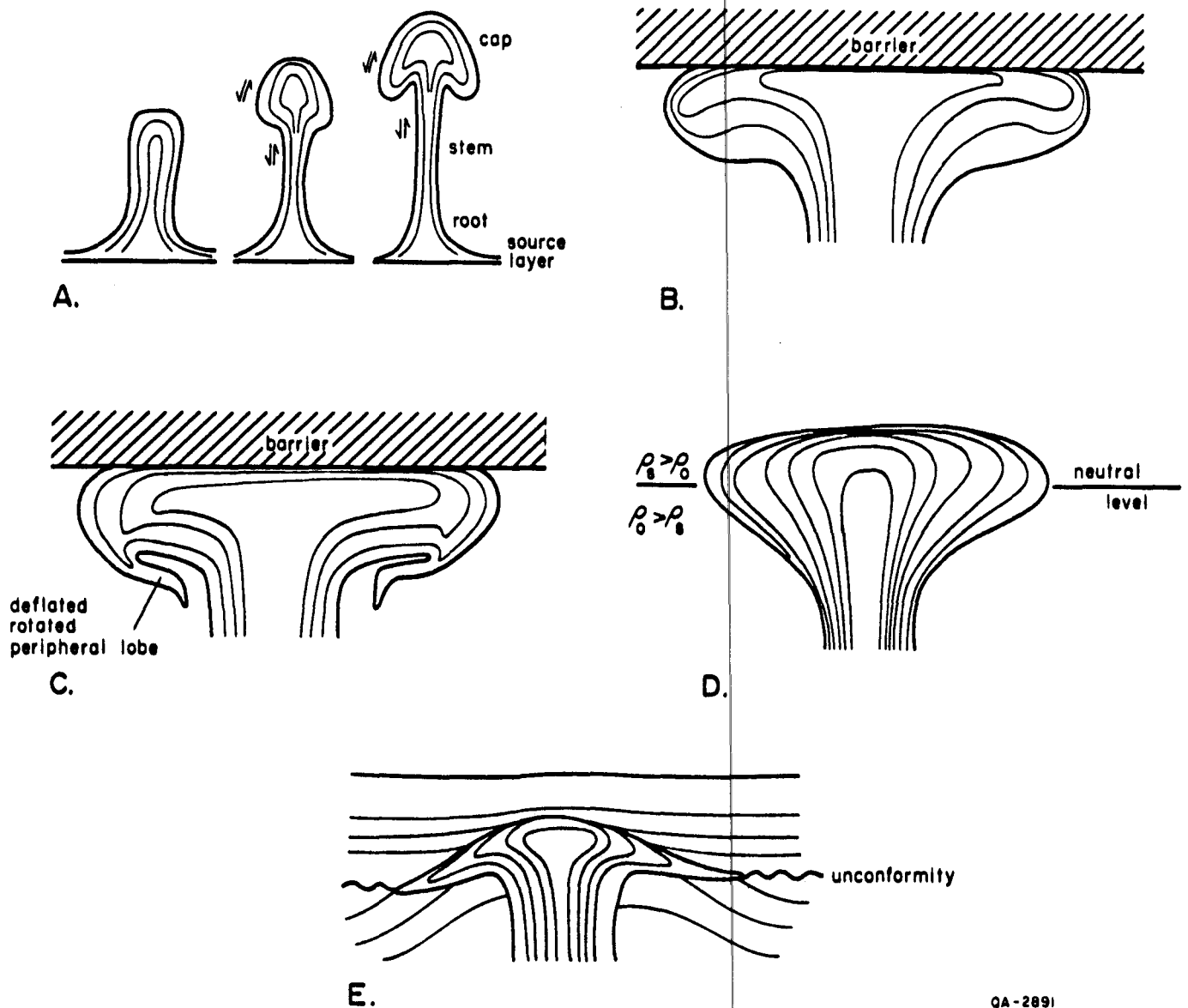
convection cells (rolls or spokes)? This question has implications to inferring dome stability.

SCOPE OF THIS REPORT

The present report is restricted to a single important aspect: internal structure of diapirs. Analysis and synthesis of the experimental data have been restricted to this aspect because of its overriding importance to understanding the host medium of a salt-dome repository. The other aspects will be studied in 1985 using data from the experimental modeling in 1984.

FACTORS CONTROLLING THE GROWTH OF MUSHROOM-SHAPED DIAPIRS

Mushroom-shaped diapirs are those having a slender stem capped by a broad cap, the outer rim of which projects downward as a hanging peripheral lobe. The diapir contact becomes deformed in this way because of the effect of viscous drag on the internal circulation patterns of the diapir (fig. 2A). The growth of this type of cap is not initiated by a barrier like other forms of cap. For instance, a cap can also form after a diapir reaches an effectively impenetrable barrier; one whose plunging strength (Ramberg, 1981, p. 277) exceeds the buoyancy pressure of diapirism (fig. 2B). This type of barrier can modify the shape of a mushroom diapir. The hanging peripheral lobes tend to keep rising until they catch up with the rest of the retarded cap against the barrier; the lobes are squeezed flat by the pressure gradient within them and can rotate to a recumbent attitude against the base of the cap (fig. 2C). Diapir caps can also spread sideways at a much more subtle barrier, that of neutral buoyancy (fig. 2D). The lower part of the cap is less dense than its surrounding medium, whereas the upper part of the cap is denser than its surrounding medium (typically unconsolidated terrigenous clastic rocks). Lastly, diapir caps can form as a result of the burial of salt extrusions (fig. 2E).



QA-2891

Figure 2. Formation of diapir caps: (A) well below an upper boundary by internal circulation and viscous drag with sinking cover; (B) normal diapir below an impenetrable barrier; (C) mushroom diapir below an impenetrable barrier; (D) by differential buoyancy above and below a neutral level at which the density of the cover (ρ_0) equals that of the salt (ρ_s); (E) a buried salt extrusion. (From Jackson and Talbot, in preparation.)

Mushroom-shaped caps are only one of several types of cap formed by viscous drag of the sinking cover and rising stem well below an upper boundary. Theoretical and experimental studies show that the shape of the diapir cap depends largely on the parameter m , the ratio of the viscosity of the overburden divided by the viscosity of the source layer (Berner and others, 1972; Whitehead and Luther, 1975; Woidt, 1978, 1980; Heye, 1978, 1979). Three morphological types can be differentiated qualitatively as types A, B, and C. Where $m \ll 1$, relatively widely spaced type A diapirs swell only slightly to thumblike shapes (fig. 3A). Where $m \sim 1$, a pronounced, type B, mushroom-shaped cap trailing a hanging peripheral lobe develops (fig. 3B). Where $m \gg 1$, type C spherical blobs trailing only tenuous stems (like balloons on threads) rise from pronounced withdrawal basins in the source layer (fig. 3C). If it becomes detached, the cap is spherical if the overburden has Newtonian flow behavior; that is, a linear relationship between stress and strain rate. But the cap develops an elongated lower portion like an inverted teardrop if the overburden is non-Newtonian (shear thinning) like real rocks (Van Dyke, 1982, figs. 182 and 183).

Most natural salt diapirs are typically portrayed as type A, possibly because of inadequate drilling data. Boreholes close to the center of the dome are rare, so the stalk is assumed to be wider than it really is. Alternatively, the misleading effects of seismic shadow mask the region below the overhang and produce a pseudo-type A profile (Tucker and Yorston, 1973, example 13). That types B and C are more likely in nature than type A is suggested by the effective viscosities calculated for natural rocks.

Salt is one of the most intensively studied materials in rock mechanics, but our current estimates of the effective viscosity of dry rock salt vary widely from 10^{15} to 10^{20} Pa·s (LeCompte, 1965; Carter and Hansen, 1983; Heard, 1972). The effects of water on salt rheology are just beginning to be adequately explored (Spiers and others, 1984); water lowers the viscosity of salt and allows it to behave more like a Newtonian fluid.

The effective viscosities of most other rocks, especially terrigenous clastic sediments, are even less precisely known. However, beds of nearly all other lithologies except potash minerals

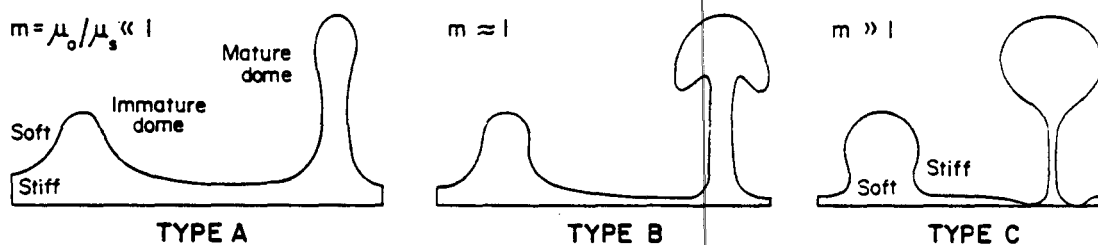


Figure 3. Schematic summary of the effects of viscosity contrast on shapes of immature and mature domes based on experimental and mathematical modeling by Berner and others (1972), Whitehead and Luther (1975), Woidt (1978, 1980), Heye (1978, 1979), and unpublished experiments at the University of Uppsala. μ_0 is the overburden viscosity and μ_s is the source-layer viscosity. Immature domes show subtle but recognizable differences that magnify with maturity. Type A: widely spaced, thumb-shaped diapirs with cap diameter only up to twice that of stem. Type B: closer spaced, mushroom-shaped diapirs with broad caps having peripheral lobes. Type C: closely spaced diapirs comprising bloblike caps trailing thin pipes of buoyant liquid and flanked by prominent peripheral sinks. (From Jackson and Talbot, in preparation.)

and bischofite fold or boudinage when incorporated in deforming rock salt. This indicates that rock salt has a lower viscosity than its country rocks. Furthermore, dynamic scaling calculations by Dobrin (1941) and Hunsche (1978) based on experimental diapirs in viscous fluids indicate that country rocks in the U.S. Gulf Coast and northwest Germany have viscosities on the order of 10^{20} Pa·s and 10^{19} Pa·s, respectively. Thus, as a working hypothesis we assume that the effective viscosity of non-evaporites is similar to or higher than that of salt. Diapir types B and C are therefore to be expected in nature.

Diapir type B with mushroom-shaped cap has the most difficult internal geometry to interpret of the three types. The infolded floor of the diapir cap is also the most threatening to a repository (see "Some implications to nuclear waste isolation), which makes it imperative to recognize and understand mushroom structures. The remainder of this report describes how such structures can be identified and analyzed on the basis of concepts developed during experimental modeling.

EXPERIMENTAL RESULTS

Figure 4 shows the starting configuration of each of the models referred to in the present report before acceleration in a centrifuge. Figure 5 shows the large number of domes produced in typical models; domes are more numerous in models simulating downbuilding than in models simulating upbuilding. This is because a smaller wavelength was encouraged in the early stages of downbuilding due to a thinner cover, as indicated by fluid mechanics theory (Ramberg, 1981, p. 90-99).

The internal structure of model diapirs is represented by layers of contrasting color in the buoyant source layer. The layers are mechanically passive, being made of the same material apart from small additions of colored powder; they do not perturb the local strain pattern and act merely as markers.

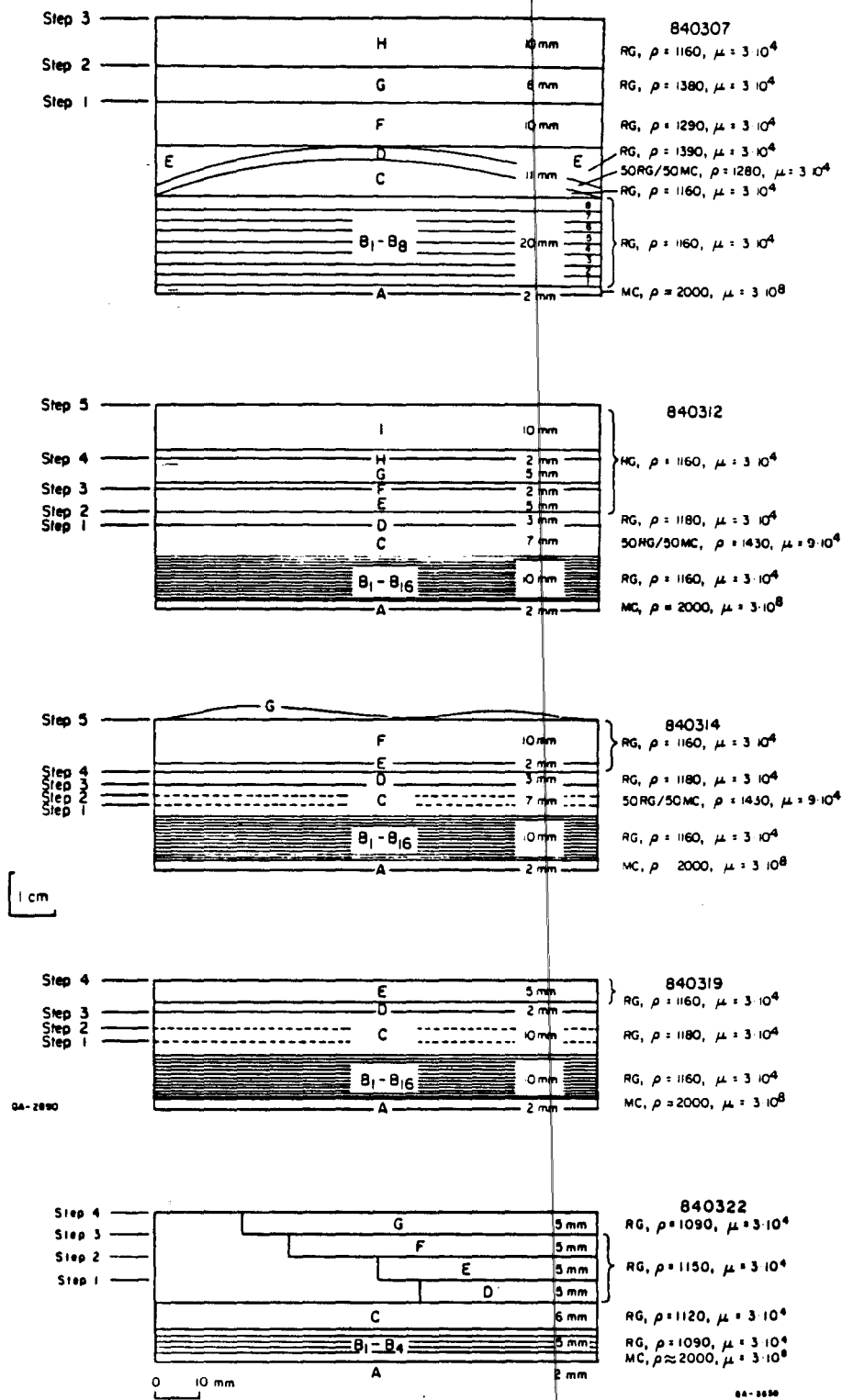
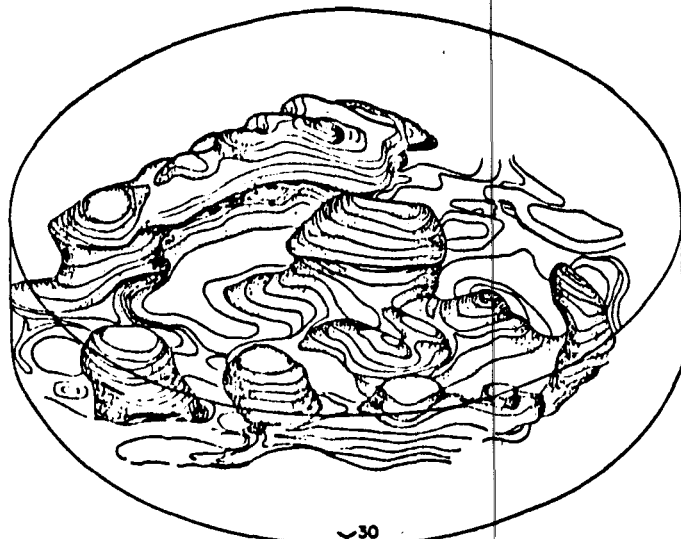
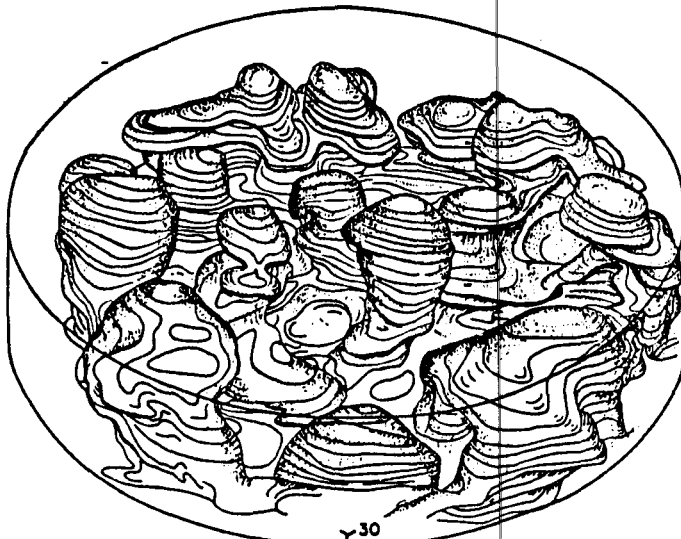
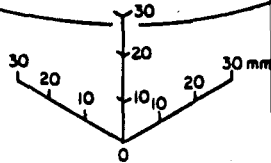


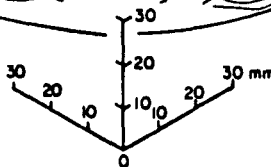
Figure 4. Starting configuration of five models before acceleration in the centrifuge. Steps refer to levels in model at which new layers were added in increments between centrifuging during downbuilding experiments. Model diapirs in 840307, 840312A, 840314B, 840319A, and 840322 grew by downbuilding; diapirs in 840312B, 840314A, and 840319B grew by upbuilding. Full details of each experiment are listed in appendix 1. ρ is density ($\text{kg} \cdot \text{m}^{-3}$), μ is effective dynamic viscosity ($\text{Pa} \cdot \text{s}$), RG is silicone putty, MC is modeling clay, 50 RG/50 MC is a mixture of 50 wt.% RG and 50 wt.% MC; densities were increased by adding BaSO_4 powder.



B.



A.



GA-2889

Figure 5. Block diagrams in isometric projection showing the number of domes produced in two similar experiments. The two models contained layers of identical properties, but 840319A was produced by downbuilding and 840319B was produced by upbuilding. The downbuilt model produced about twice as many domes as did the upbuilt model.

GENERAL ANATOMY OF MUSHROOM STRUCTURES

The internal geometry of even the simplest model dome is complex. Infolded overhang floors, downfolded peripheral lobes, spurs, vortices, and multistalked and multicapped diapirs have been recognized. In the absence of any published scheme of nomenclature for such complex structures, a comprehensive system of concepts and nomenclature was jointly developed by the present authors, published in Jackson (1984), and is expanded here.

In the schematic symmetrical mushroom diapir (fig. 6), flow of material within the diapir can be traced by the orientation of the major internal folds. The folds are defined by bedding equivalent to anhydrite layers in natural salt stocks. Salt rises up the core of the structure to its crest before flowing laterally as a sidefold, then downward at the margins as a downfold. Between the peripheral downfold and the core is a circular, elliptical, or crescentic infold of cover material. The top of the diapir is defined by the crestfold.

Apart from the infold, which is synclinal, all the folds defined in the previous paragraph are anticlinal, having the oldest strata in their cores. However, both the infold and downfold are downward-facing folds. (A fold faces in a direction normal to its axis, along the axial surface, and toward the younger beds.) Thus the downfold and infold are a synformal anticline and an antiformal syncline, respectively. Figure 6 shows the formal terminology based on these relationships in which the structures can be referred to by their acronyms as AAC, CAA, CRA, PSA, and IAS. The tripartite compound name describes the shape of the fold (antiformal, synformal, neutral), its relation to the stratigraphy (anticline, syncline), and a description of its location in the diapir or dominant characteristic (core, crestal, peripheral, infolded, reversed). Note that the PSA downfold can be traced without discontinuity into the AAC core via the CRA.

These names describe the type of major folds within model or natural salt diapirs. The number of major folds is also used to classify diapirs. Both diapirs shown in figure 7 would yield vertical sections like that in figure 6, but their horizontal sections are quite different.

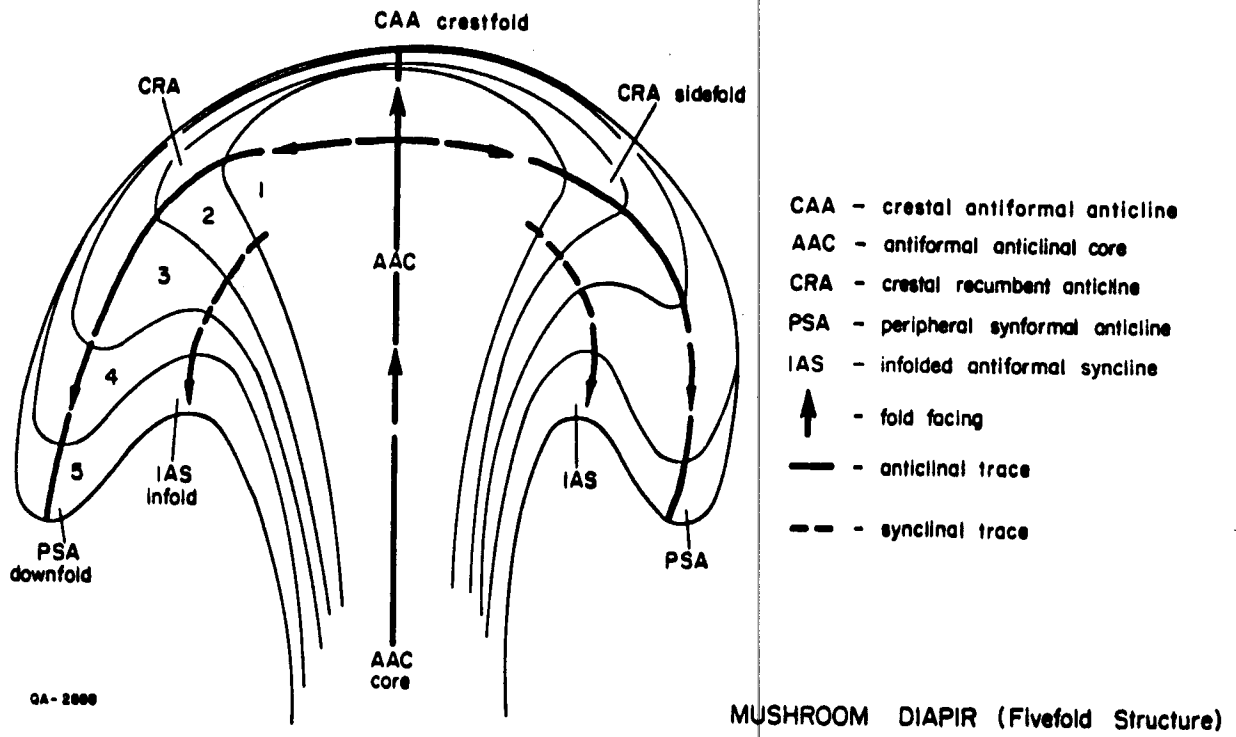


Figure 6. Schematic symmetric fivefold mushroom diapir in vertical section showing terminology of major folds.

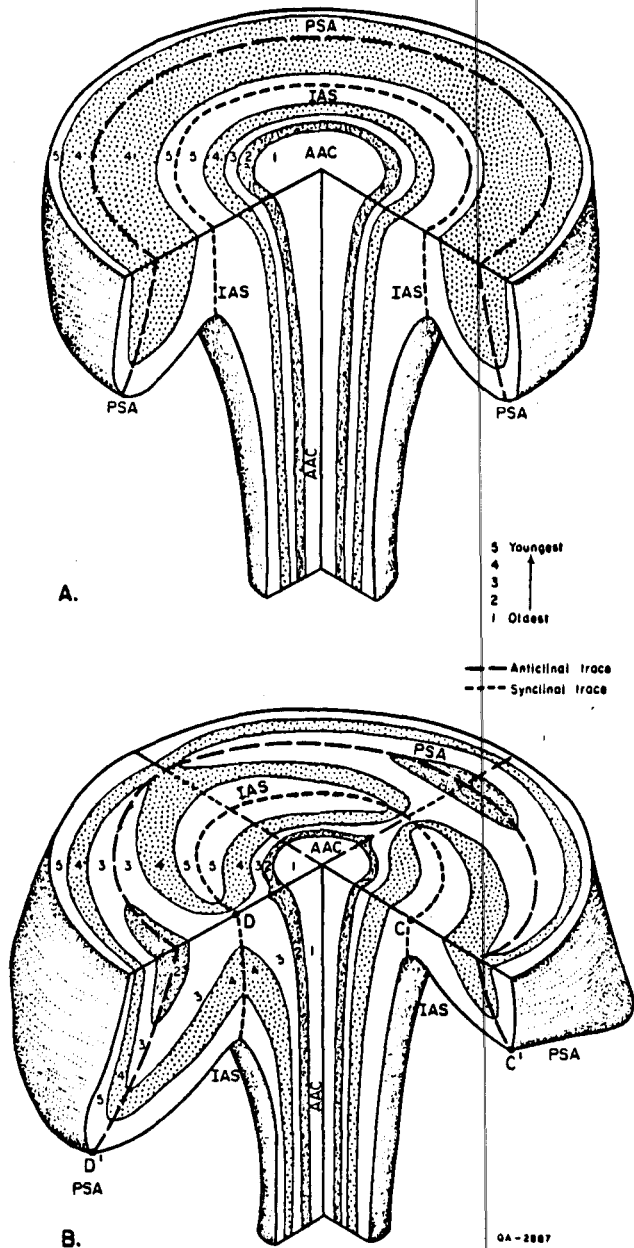


Figure 7. Block diagrams of schematic fivefold diapirs to show relation between vertical sections (similar to fig. 5) and horizontal section. A, axially symmetric diapir cut along any two of the infinite orthogonal planes of symmetry. B, orthorhombic symmetric diapir cut along the two planes of symmetry, which also correspond to the axial planes of two major radial folds. Orthorhombic symmetry results from PSA and IAS being greater in amplitude in opposite sectors than in adjacent sectors. Points D and D' mark the depression points of the PSA and IAS, whereas C and C' mark the culmination points of these folds.

Figure 7A shows a schematic horizontal cross section through an axially symmetric diapir; any traverse line across the center of this section would intersect five major axial traces. Both the PSA and IAS would be intersected twice because these are peripheral structures encircling the diapir; the core would also be intersected. This structure is therefore called a fivefold diapir. Figure 7B shows a fivefold diapir that has orthorhombic symmetry about two vertical planes rather than about an axis. The PSA is larger on two opposite sectors of the diapir than in adjacent sectors where the IAS is larger. The crescentic closed fold structures in figure 7B characterize horizontal cross sections through diapirs that are not precisely axially symmetric, that is, virtually all natural salt domes.

However, not all horizontal cross sections through axially asymmetric diapirs will contain crescentic fold patterns. Shapes in cross section depend on the structural level within the diapir. A horizontal section through the CAA crestfold above the axial trace of the CRA (fig. 6) will show only a simple dome, represented by a concentric target pattern. The same pattern characterizes a section through the AAC diapir stalk. As is demonstrated in the following section, horizontal sections at different levels of the diapir cap yield profoundly different fold patterns, a fact that the interpreter must constantly bear in mind.

The basic major folds that appear in most sections (AAC, IAS, and PSA) are instantly recognizable in vertical cross section. However, their identification in horizontal section requires careful interpretation. If the internal stratigraphy is known, as is the case for all model diapirs and natural ones with potash beds and reliable way-up structures, anticlines can be differentiated from synclines by having the older beds in their core. In the absence of a known stratigraphy, major folds must be recognized by comparing their patterns to model and natural diapirs with known stratigraphy. Differentiation between the AAC and the PSA requires care, for both these anticlines can merge in horizontal and vertical sections (figs. 6 and 7). Both have older units in their cores, but the AAC invariably has the oldest unit in the section. As will be shown in the next section, the AAC core can be located either in the center or near the periphery of a diapir in horizontal section, so its location does not assist in its identification.

SPECIFIC ANATOMY OF MODEL MUSHROOM DIAPIRS

This section illustrates and interprets diapirs of increasingly complex internal structure. Almost all models were sectioned both horizontally and vertically. But it is impossible to cut complete vertical and horizontal sections through the same diapir. Thus, if we wish to illustrate a structure in both these orientations, we either have to graphically construct a section normal to that in a model slice or find a perpendicular section through a different dome in the same model that resembles the dome in the original slice. In the diagrams that follow, sections through real models are identified as such by the model number next to them; constructed sections are recognized by the absence of a model number.

The boundary conditions control the symmetry of model diapirs. Those grown near the edges of the model are almost invariably asymmetric and tilted toward the center of the model. This configuration results because of the drag exerted on flowing materials by the walls of the centrifuge cup. Diapirs grown near the center of the model tend to be more symmetric (tending toward orthorhombic or axial symmetry) and vertical, unless distorted by the influence of a large neighboring diapir. "Near" and "far" on figures refer to the proximity of the model center. Thus, each model provides diapirs in a range of styles to study (fig. 8).

Threefold Diapirs

All threefold diapirs are asymmetric (fig. 9). The AAC core is located near the edge of the structure, their PSA downfold on the opposite side, and their IAS infold in the middle. In figure 9 the PSA has been dragged both downward and inward by flow of the cover beneath the overhang of the cap.

Fivefold Diapirs

Figure 10 shows an asymmetric fivefold diapir in vertical section and in three horizontal sections at different structural levels. The central horizontal section shows fivefold structure, those above and below show threefold structure, and those above and below these (not illustrated) show onefold structure. The AAC core changes position between the two threefold

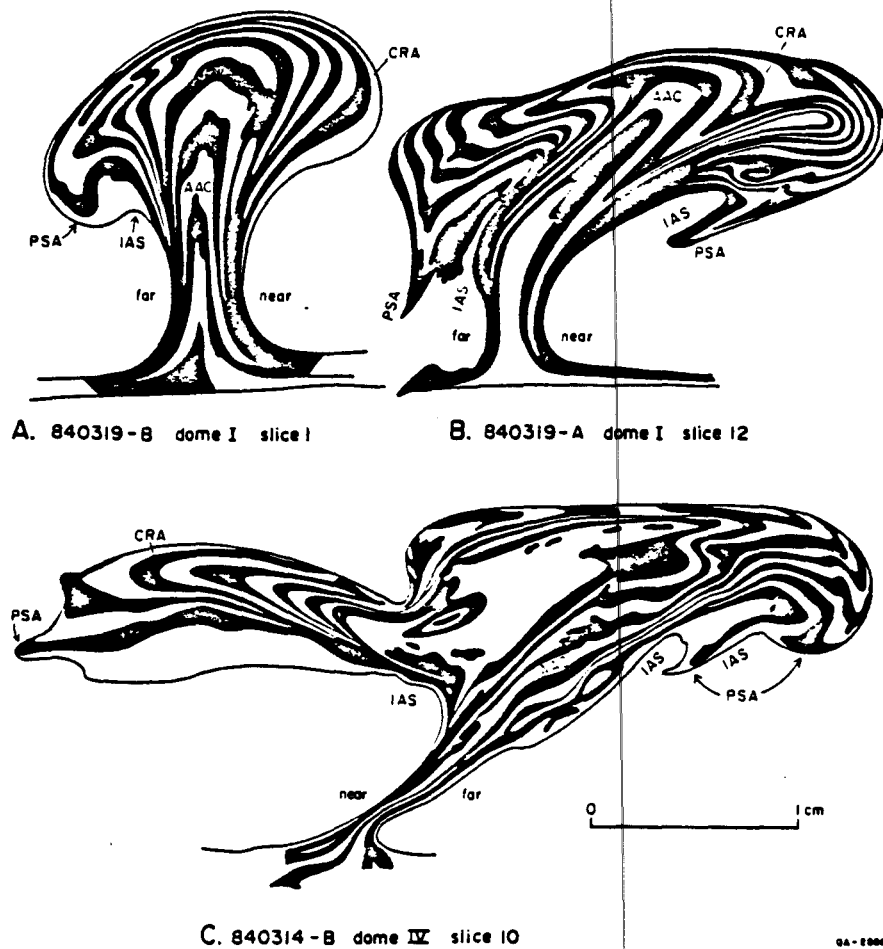
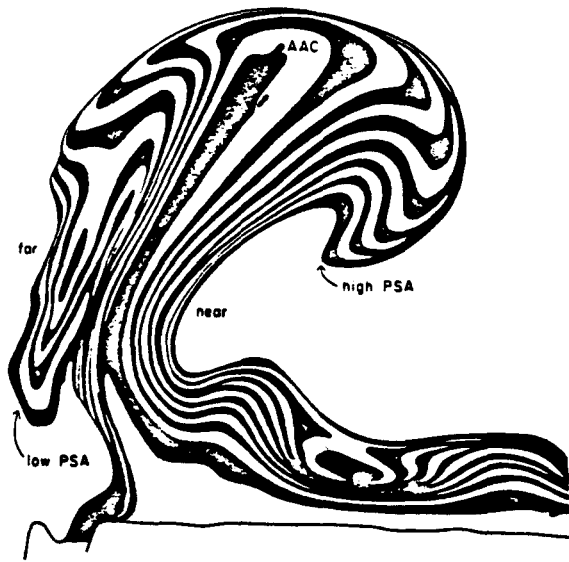
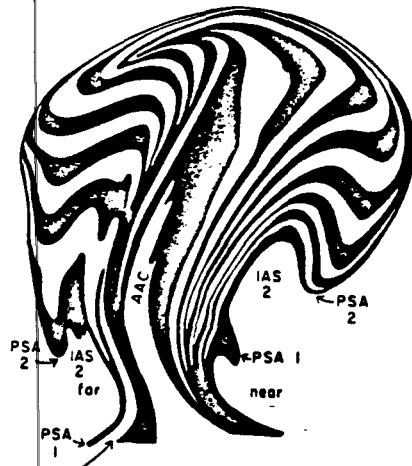


Figure 8. A variety of model domes in vertical section. Alternating black and white layers are passive markers of identical mechanical behavior.

- A, Asymmetric diapir with PSA and IAS on left side and simple overhang on right side.**
- B, Asymmetric diapir with preferential tilt of stalk toward model center (near side); cap equally developed on each side.**
- C, Asymmetric diapir with preferential tilt of stalk; unusually large breadth of cap results from section passing through diapir wall along circumferential boundary; cap overhang greater on far side.**

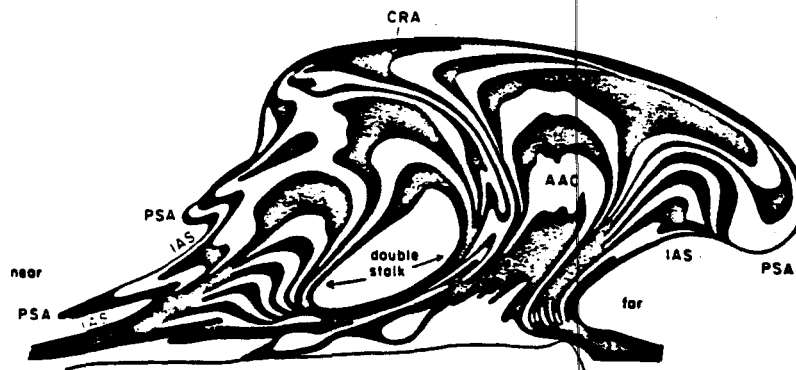


D. 840319 - A dome I slice 1



E. 840319 - A dome I slice 2

0 1 cm



F. 840319 - A dome IV slice 10

GA-1006

Figure 8 (continued)

- E, Double spurs or lobes on each side, the left lobe 1 being greatly flattened by inward flow of cover toward diapir stem. Each lobe was produced by flattening of the diapir by one load increment, which formed a shoulder on the diapir; the shoulder was then sheared by sinking cover to produce a peripheral lobe.
- F, A rare example of diapirs tilted away from the model center (to far side), two diapirs fused to form a single cap over a double stalk; the right diapir cap extends over the left diapir.

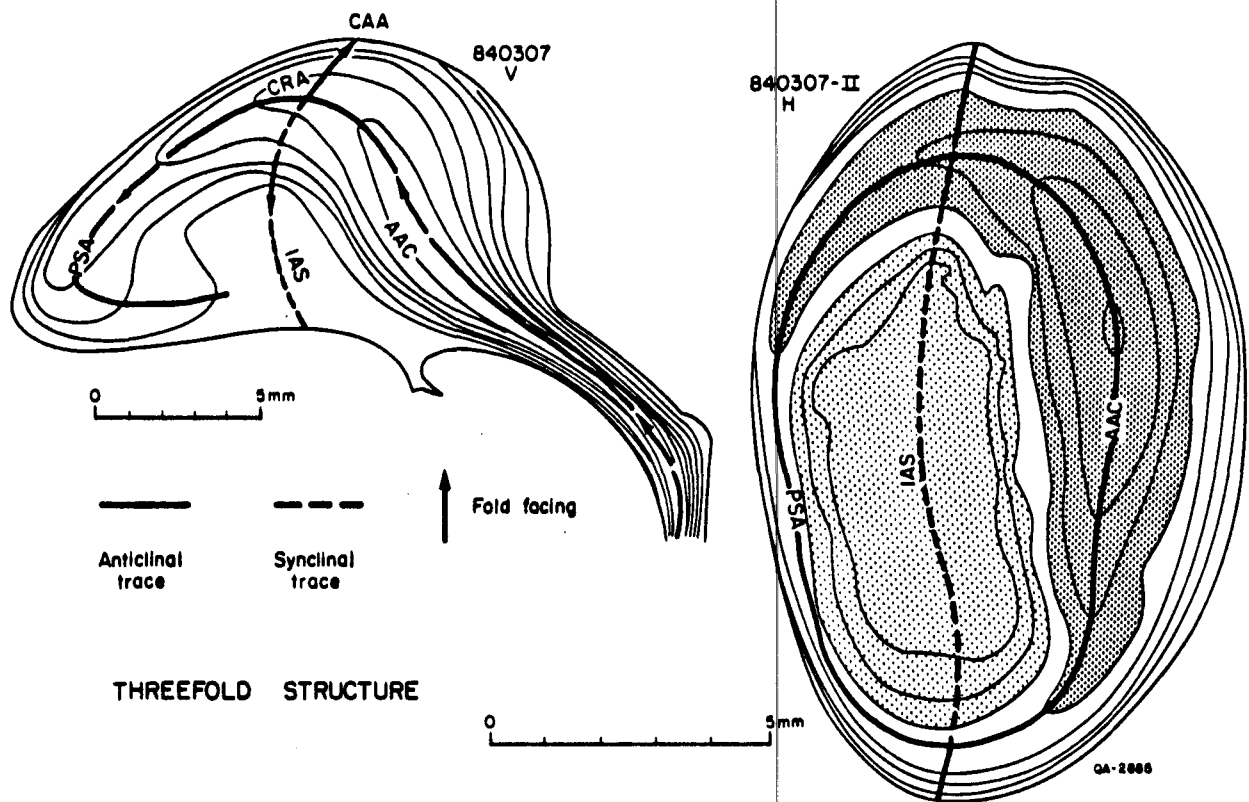


Figure 9. Vertical (V) and horizontal (H) sections through threefold asymmetric model diapirs. Arrows show fold facing. AAC, antiformal anticlinal core; CAA, crestal antiformal anticline; CRA, crestal recumbent anticline; PSA, peripheral synformal anticline; IAS, infolded antiformal syncline.

FIVEFOLD
STRUCTURE

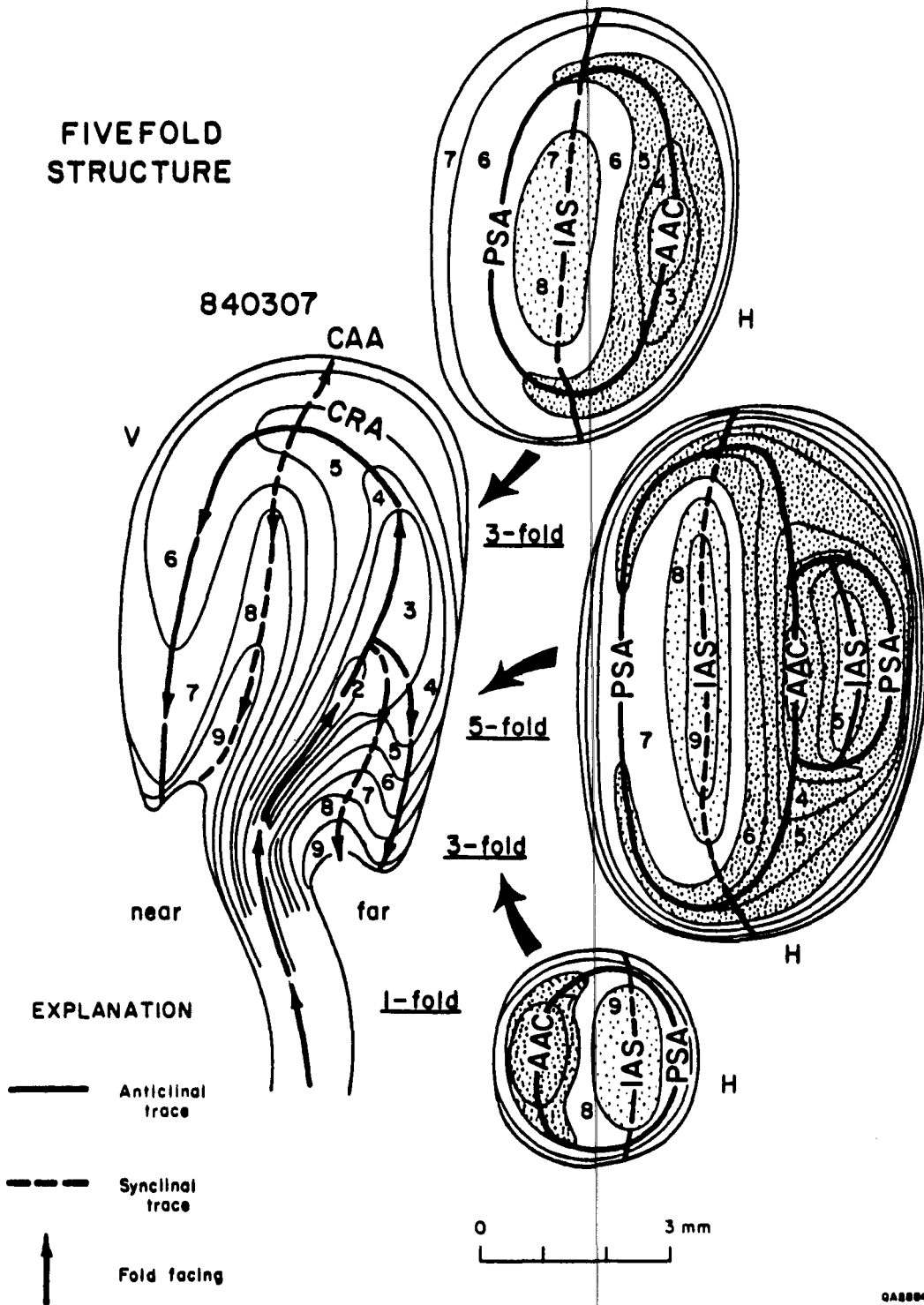


Figure 10. Vertical (V) and horizontal (H) sections through a fivefold asymmetric model diapir. Horizontal sections are drawn at three different structural levels. Numbers show stratigraphic sequence; arrows show fold facing. AAC, antiformal antidual core; CAA, crestal antiformal anticline; CRA, crestal recumbent anticline; PSA, peripheral synformal anticline; IAS, infolded antiformal syncline.

structures. The central fivefold level is the most complex. Two crescents arranged back-to-back represent the AAC. The arms of the crescents merge into two different PSAs, which encircle two different IASs. This section also illustrates another general rule of interpretation: the outermost concentric folds in diapirs are invariably anticlines.

Sevenfold Double Diapirs

Sevenfold diapirs can be produced in at least three ways: (1) by two increments of loading by the overburden, which produce a double pair of PSAs and IASs, as in figure 8E; (2) by a double overturn of the diapir interior to form a vortex (next section); and (3) by a double diapir (this section).

Double diapirs most commonly form by lateral fusion of the caps of two similar diapirs. Fusion is common where diapirs are growing by downbuilding, because the dominant wavelength of diapirism lengthens in response to the increasing thickness of cover. The result is two distinct diapir stalks and a single cap with sevenfold internal structure overall (fig. 8F). Each stalk is separated by a core of cover defining an antiformal synclinal core (ASC) and a synformal synclinal core (SSC) (fig. 11). Note that the cover rock ASC projects deep into the diapir cap.

Double diapirs form less commonly by the noncoeval growth of dissimilar diapirs, giving rise to a structure resembling a human arm draped across a head in vertical section (fig. 12). This structure arises after an older asymmetric diapir spreads laterally over a younger or slower diapir. The younger diapir continues rising, thus arching and stretching the older diapir over the crest of the younger diapir. By analogy, the older diapir is the arm and the younger diapir, the head. Between the two diapirs is a pinched zone of cover material of variable thickness extending into the heart of the double structure. This pinched IAS is downward facing near the periphery of the double diapir, as is common in other types of diapir, but is upward facing near the center of the structure.

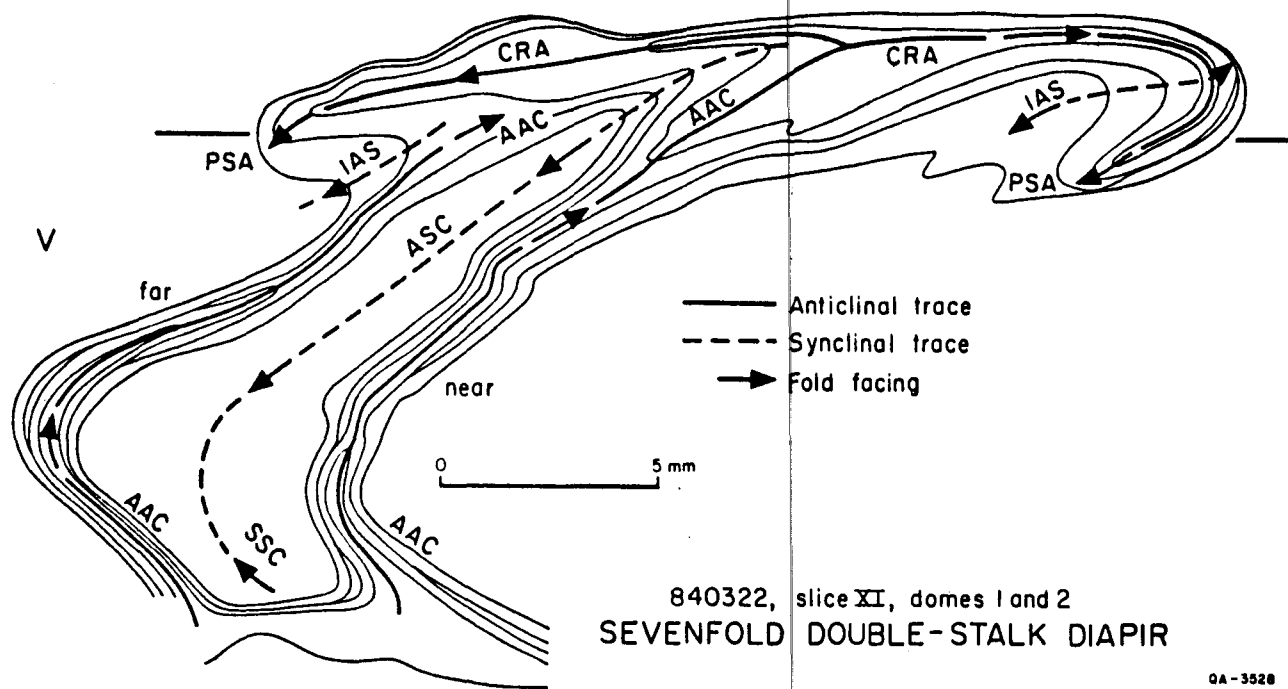


Figure 11. A sevenfold double-stalk diapir formed by lateral fusion of the caps of two coeval model diapirs. A core of cover rock defines the antiformal synclinal core (ASC) and the synformal synclinal core (SSC). The ASC projects into the center of the cap. AAC, antiformal anticlinal core; CRA, crestal recumbent anticline; IAS, infolded antiformal syncline; PSA, peripheral synformal anticline.

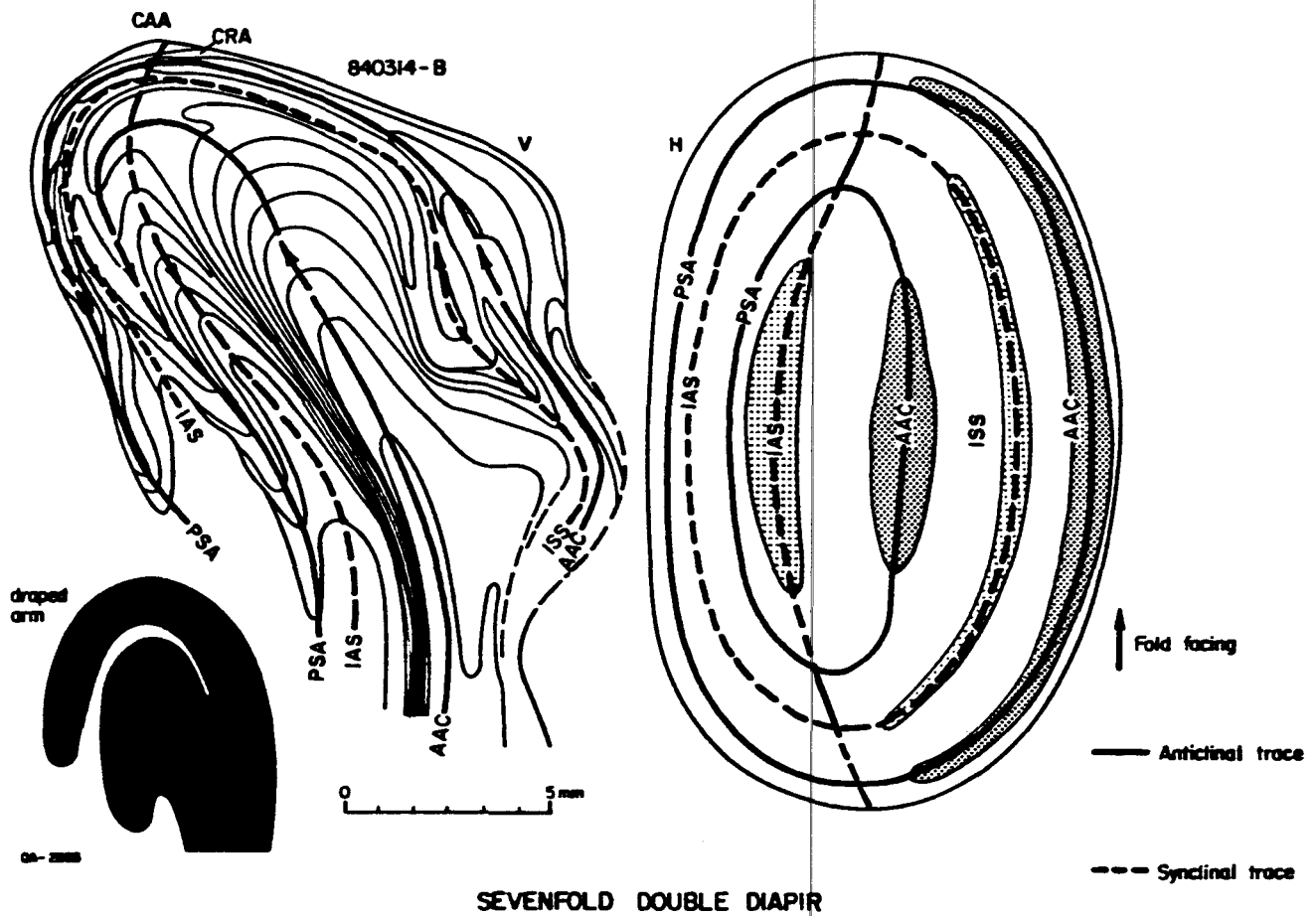


Figure 12. Vertical (V) and horizontal (H) sections through a sevenfold asymmetric double diapir with a draped-arm structure shown schematically below. Arrows show fold facing. AAC, antiformal anticlinal core; CRA, crestal recumbent anticline; PSA, peripheral synformal anticline; ISS, infolded synformal syncline; IAS, infolded antiformal syncline.

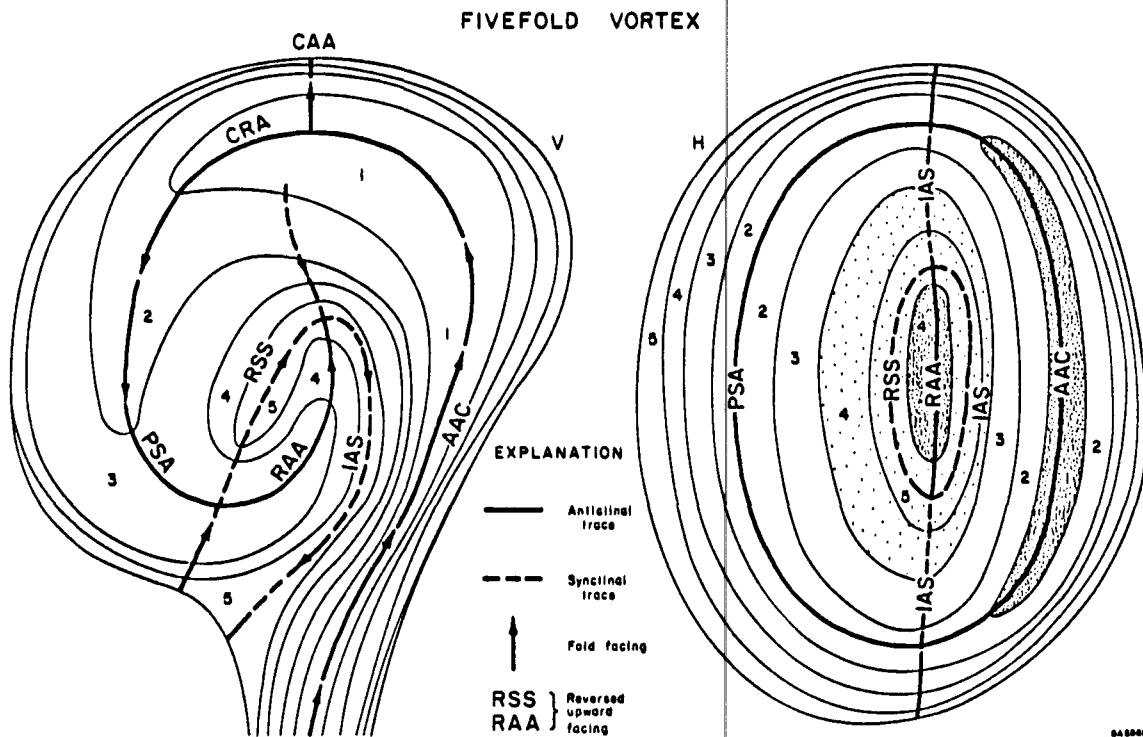


Figure 13. Vertical (V) and horizontal (H) sections through a schematic fivefold asymmetric diapir with vortex structure. Numbers show stratigraphic sequence; arrows show fold facing. AAC, antiformal anticlinal core; CAA, crestal antiformal anticline; CRA, crestal recumbent anticline; IAS, infolded antiformal syncline; PSA, peripheral synformal anticline; RAA, reversed antiformal anticline; RSS, reversed synformal syncline.

Vortex Structures

Vortex structures can form adjacent to the core of a diapir if there is more than one overturn of the diapiric material. The first overturn produces downward-facing folds such as the typical PSA and IAS. A second overturn refolds these downward-facing folds back into an upward-facing orientation. The resulting structures are termed "reversed upward facing" to distinguish them from upward-facing structures like the AAC core that have not overturned even once.

Figure 13 is a schematic fivefold vortex in vertical and horizontal section. It is a modified version of figure 9, a simple threefold diapir. Structures in the center of the cap are reversed upward facing. If a fivefold structure becomes rolled up by vorticity, a ninefold vortex structure could form, but such a structure has not yet been recognized in the model diapirs. It is also possible for a fivefold diapir to develop a vortex on one side only, giving rise to a sevenfold vortex structure (fig. 14).

Vortex structures are well known in thermal convection (Rayleigh-Bénard instability) and in buoyancy diapirism due to density inversion (Rayleigh-Taylor instability) with high Reynolds numbers (inertial forces greater than viscous forces). However, neither of these conditions applies to the experimental diapirs, and vortex structures have not been previously reported in centrifuge models. In the present case, vorticity arises not by inertia but because of viscous drag. Movement of the sinking cover forms the PSA downfold by retarding the rise of the PSA relative to the AAC core. The diapir cap expands sideways, and as a result the sinking cover begins to move inward under the overhang of the cap. Viscous shear by the cover rotates the PSA inward as well so that it becomes recumbent. The innermost part of the recumbent PSA then enters the drag zone of the rising AAC and, as a result, is sheared upward by the rising diapir stalk, rolling up to form a vortex.

MUSHROOM DIAPIRS IN NATURE

The model diapirs interpreted in the previous section are highly suitable to analyze because

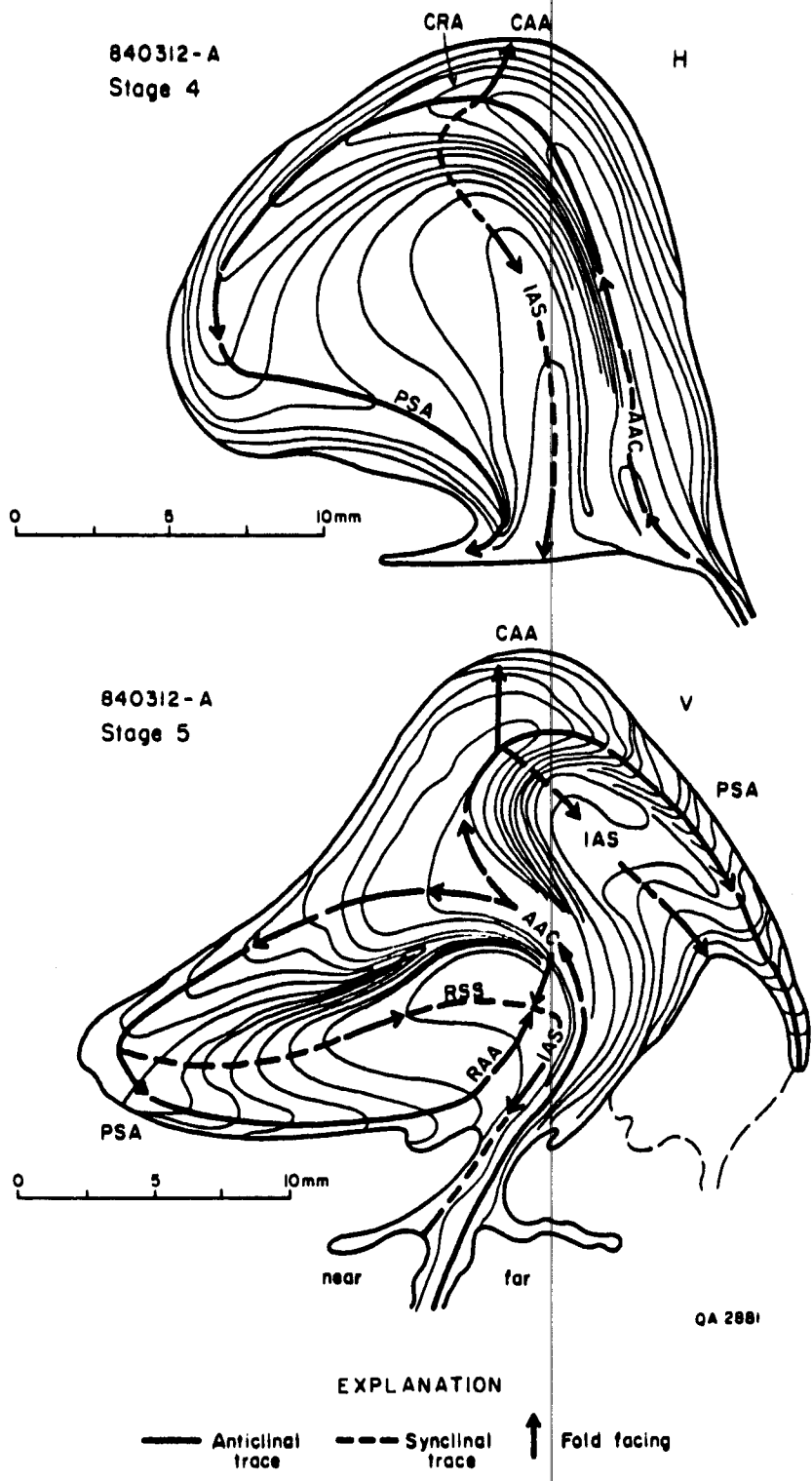


Figure 14. Vertical sections through two model diapirs at different stages of development. Top, immature threefold asymmetric diapir. Bottom, mature sevenfold asymmetric structure showing vortex structure in left half. Arrows show fold facing. AAC, antiformal anticlinal core; CAA, crestal antiformal anticline; CRA, crestal recumbent anticline; IAS, infolded antiformal syncline; PSA, peripheral synformal anticline; RAA, reversed antiformal anticline; RSS, reversed synformal syncline.

1. The geometry and sequence of all units in the predeformational state are known (fig. 4), which allows reliable correlations of marker layers after deformation.
2. The sequence of deformation (kinematics) is observable or easily inferred.
3. The three-dimensional geometry of complex structures formed during diapirism is known by slicing the model at the end of the experiment. Natural salt diapirs have few of these advantages, so it becomes essential to apply the lessons learned in analyzing model diapirs.

The nearest natural analogs to the sliced model domes are diapirs exposed at surface in arid or arctic areas where evaporites are not readily dissolved or covered by thick surficial deposits or dense vegetation. This section reviews three locations in which natural evaporite diapirs contain folds recognizable as mushroom structures on the basis of their experimental analogs.

Canadian Arctic Islands

Exposed diapirs in the Sverdrup Basin of the Canadian Arctic (Tozer and Thorsteinsson, 1964; Schwerdtner and Osadetz, 1983) consist mainly of anhydrite with nonevaporite inclusions and rare halite (fig. 15A). Barrow Dome contains a well-defined crescent of mafic plutonic rocks similar in shape and position to those in the model diapirs. Radial folds predominate inside this crescent, and concentric folds predominate outside it. Insufficient structural and stratigraphic data are provided for this dome to be reliably interpreted, but some suggestions can be made.

Figures 15B through D show successive stages of emplacement of evaporites and country rock to form a composite diapir by the process known as balloon tectonics. Conceivably, this process could form the crescent shown in figure 15A, but it is most unlikely that a crescent of mafic plutonite could be emplaced diapirically in the manner shown, for the rock is too dense. This hypothesis can therefore be rejected.

It is likely that the crescent of mafic plutonite represents deformed country rock, probably overlying the original evaporite source layer. On the basis of the radial and concentric

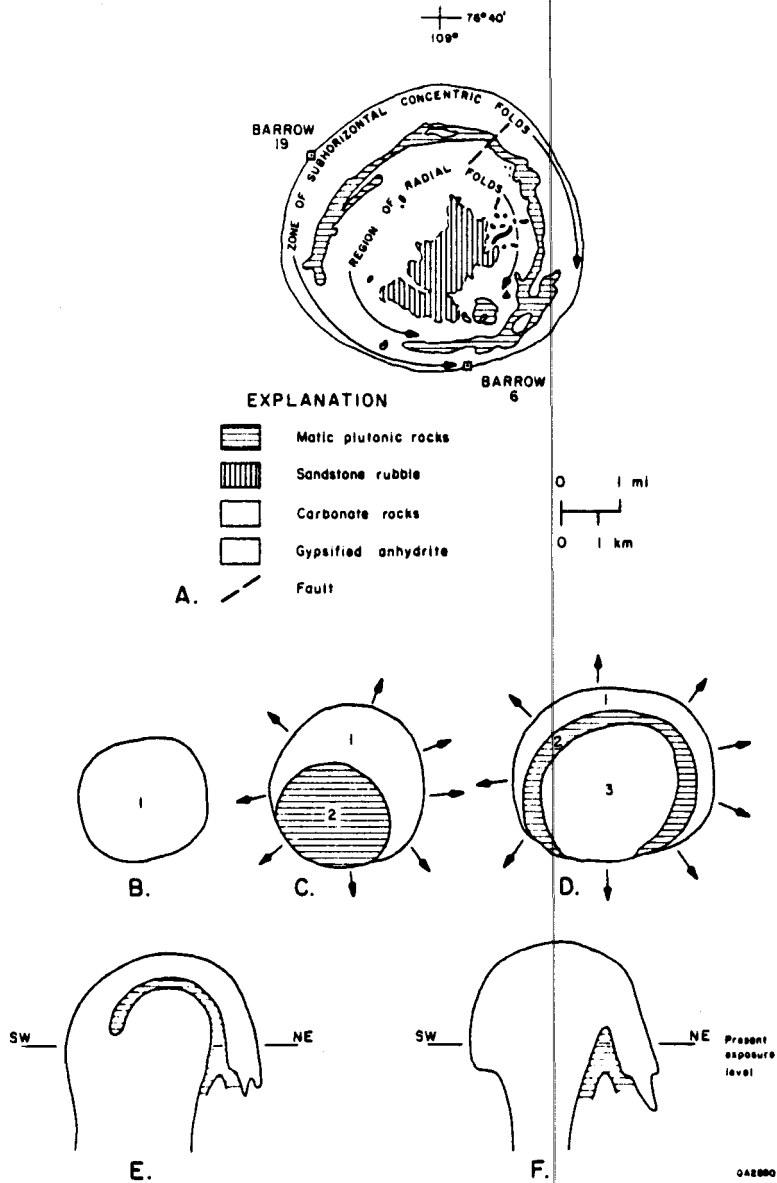


Figure 15. Barrow Dome, an exposed composite diapir of gypsified anhydrite-mafic plutonite in the Sverdrup Basin, Arctic Canada. A, map of dome from Tozer and Thorsteinsson (1964) and Schwerdtner and Osadetz (1983). B, C, D, an unrealistic model for the composite diapir in terms of balloon tectonics viewed in horizontal section. E, F, more realistic models in vertical section in which the mafic plutonite represents an infolded antiformal syncline or an infolded synformal syncline of cover rock.

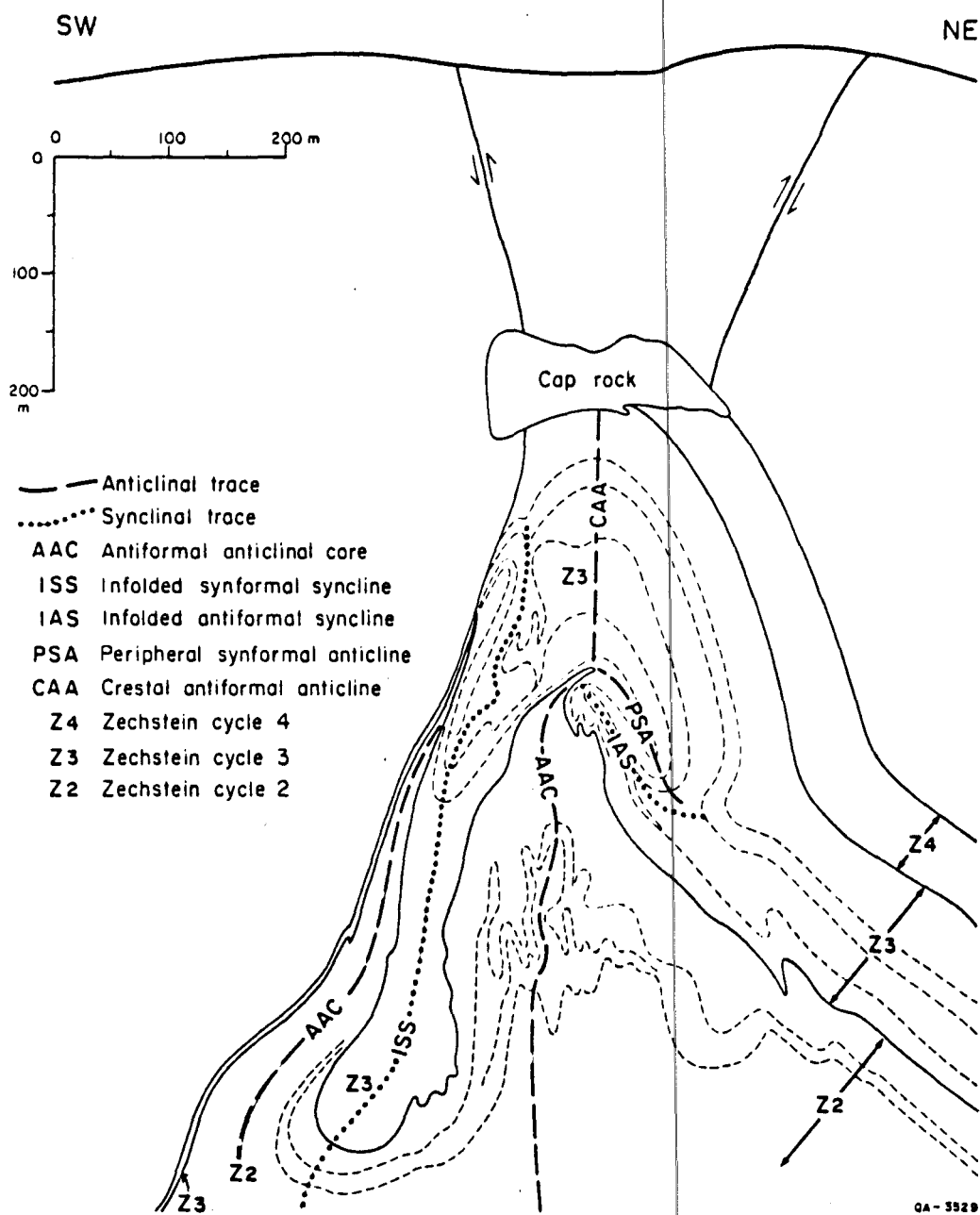


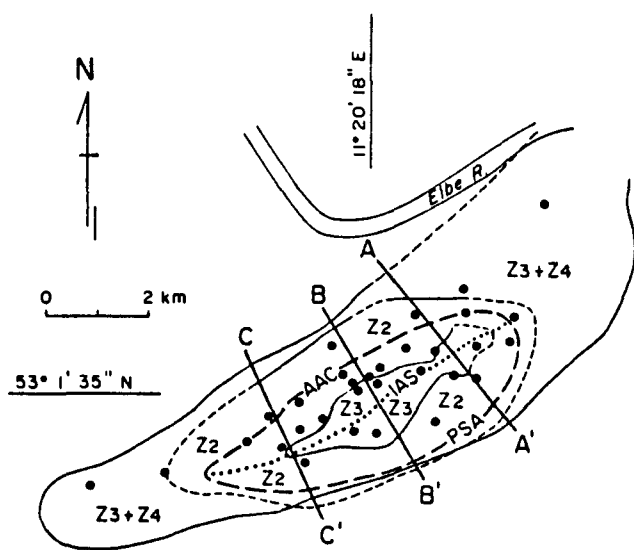
Figure 16. Cross section of Asse Dome, West Germany. Extensive mine workings omitted for clarity. First-order folds define a fivefold double diapir; the inner part is a threefold asymmetric diapir. A major ductile shear zone has telescoped or removed some Zechstein and younger units on the SW side. (Adapted from Essaid and Klaar, 1982.)

folds, we hypothesize that the crescent represents a pinched infold of country rock between diapiric evaporites, as shown in the cross sections (figs. 15E and 15F). Both these sections show the crescent as younger material being drawn in from below the diapir cap. Analogy with the models suggests that the inner area of radial folds represents an AAC core, whereas the outer area of concentric folds represents a PSA downfold.

Northwest German Plain

At least two salt domes in West Germany show internal mushroom structures comparable with those modeled. Both domes are highly elliptical, intermediate in shape between a salt stock and a salt wall, and are or might be used for storage of radioactive wastes. Asse Dome (fig. 16) has been mined for potash and salt for more than 90 years and is currently being used for storing low-level nuclear waste. Extensive multilevel mining operations (the effects of which have been omitted from figure 16 for clarity) have revealed the first- and second-order folds depicted. The first-order folds define a fivefold double diapir (two AACs), the innermost of which has a threefold asymmetric structure with a well-defined downward-facing PSA and IAS. The infolded synformal syncline (ISS) comprises evaporites of the Zechstein cycle 3 in the Asse Dome but also comprises cover material in the model dome shown in figure 12. The crest of the Asse Dome is the crestal antiformal anticline (CAA).

Gorleben Dome (fig. 17) is being considered as a possible site for storage of West German high-level nuclear waste. In each of the three cross sections the first-order folds (AAC, IAS, and PSA) clearly define an asymmetric threefold diapir comparable to the model diapir shown in figure 9. The existence of downward-facing folds (here called the IAS and PSA) was recognized by Bornemann (1982). But this geometry has important implications that are not mentioned in Bornemann's paper; they are discussed in the present paper in the section "Some implications to nuclear waste isolation." Note that in cross section C-C' (fig. 17) the IAS is known to be cored by evaporites of the Zechstein cycles 3 and 4. However, in the other two cross sections, drilling has been too shallow and widely spaced to determine whether the IAS is cored by the Zechstein



- A ——— A' Line of section
 I • Borehole
 ——— Contact, known
 ····· Contact, inferred by Bornemann (1982)
 - - - Contact, inferred in present paper
 - - - Anticlinal trace
 ····· Synclinal trace

- AAC Antiformal anticlinal core
 IAS Infolded antiformal syncline
 PSA Peripheral synformal anticline
 CAA Crestal antiformal anticline

STRATIGRAPHY

CR	Country rock
Cap rock	Cap rock
Z4	Zechstein cycle 4
Z3	Zechstein cycle 3
Z2	Zechstein cycle 2

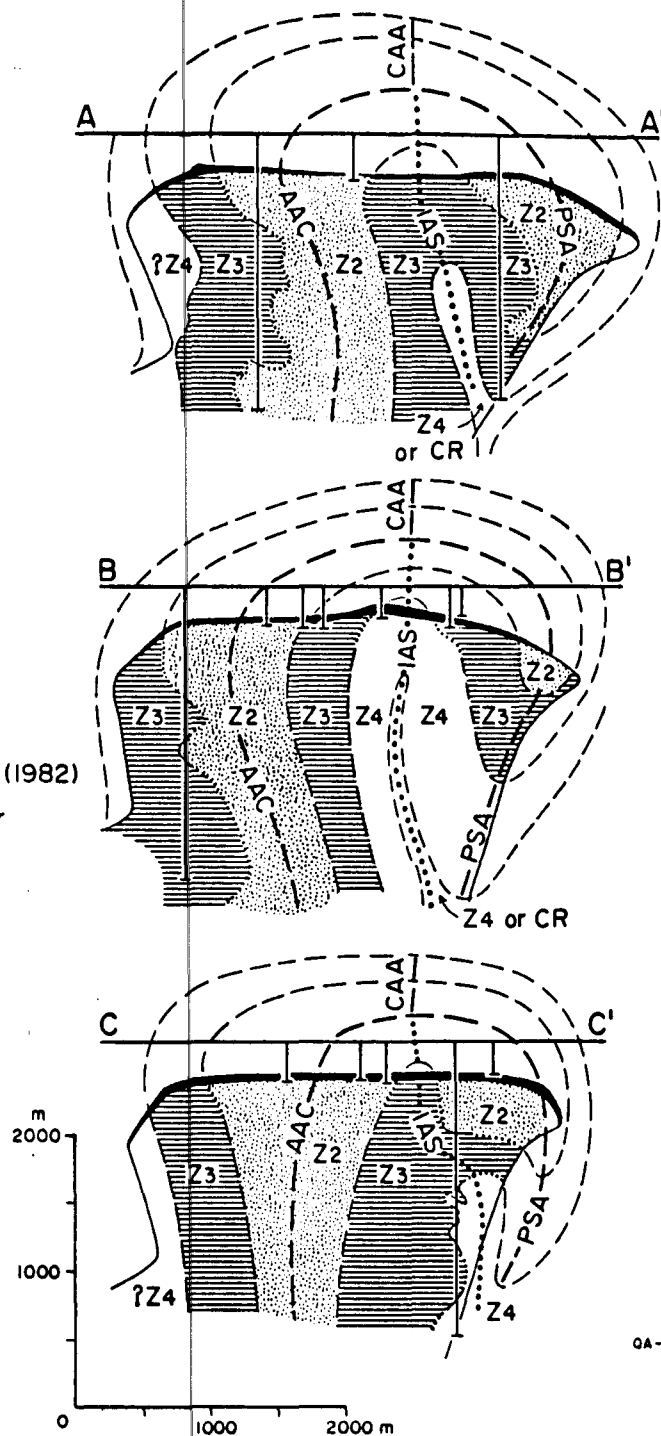


Figure 17. Map (left) and three cross sections (right) of Gorleben Dome, West Germany. The dome is a threefold asymmetric diapir. Units shown in the cross sections of Bornemann (1982) have been extrapolated to show the overall structure of the dome before the sides and crest of the dome cap partly dissolved. (Adapted from Bornemann, 1982).

evaporites or by country rock. This uncertainty is of the utmost importance to the integrity of a hypothetical repository in the center of the dome.

U.S. Gulf Coast

Salt diapirs in the U.S. Gulf Coast differ from the German domes in two main respects: They generally do not contain readily correlatable internal layers because of the purity of their constituent rock salt, and they are not exposed at the surface. Nevertheless, at least one dome--the Palangana Dome of South Texas--can be recognized to have a mushroom structure. Exploration for potash minerals, which provide a basis for internal stratigraphic correlation, during the 1950s provided unusually useful subsurface data on internal structure by means of clusters of deviated boreholes (Hofrichter, 1968). Four lithostratigraphic groups (Anhydritic, Benavides, Palangana, and San Diego) constitute the internal stratigraphy, two of which contain markers in the form of potash beds. Hofrichter and his co-workers were not sure whether or not their stratigraphic sequence was inverted and did not attempt to analyze the diapir structure. A horizontal section prepared by Hofrichter and co-workers is shown in figure 18A and their vertical section is shown in solid lines in figure 18B. Changes in younging direction mapped by these workers indicate that at least four major folds are present in their vertical section. The simplest explanation of this structure is shown in dashed lines in figure 18B. The diapir has a structure equivalent to a fivefold, slightly asymmetric, mushroom-shaped diapir.

Many of the Gulf Coast salt domes contain exotic inclusions of shale, sandstone, or carbonate. Some of these inclusions provide indirect equivocal evidence of mushroom-shaped diapirs. Kupfer (1974) drew attention to a wall-like zone of halite containing shale inclusions constituting a boundary shear zone in Belle Isle Dome, Louisiana (fig. 19), "The boundary shear zone appears to start at the edge of the salt stock as an external shear zone and penetrate into the salt mass and disappear near the center of the salt stock." (Kupfer, 1974, p. 222) This shale zone was first mapped and dated as Frio-Anahuac (Oligocene) age by Paine and others (1965). The Louann Salt in the crest of Belle Isle Dome, which has risen 12 to 15 km from its source

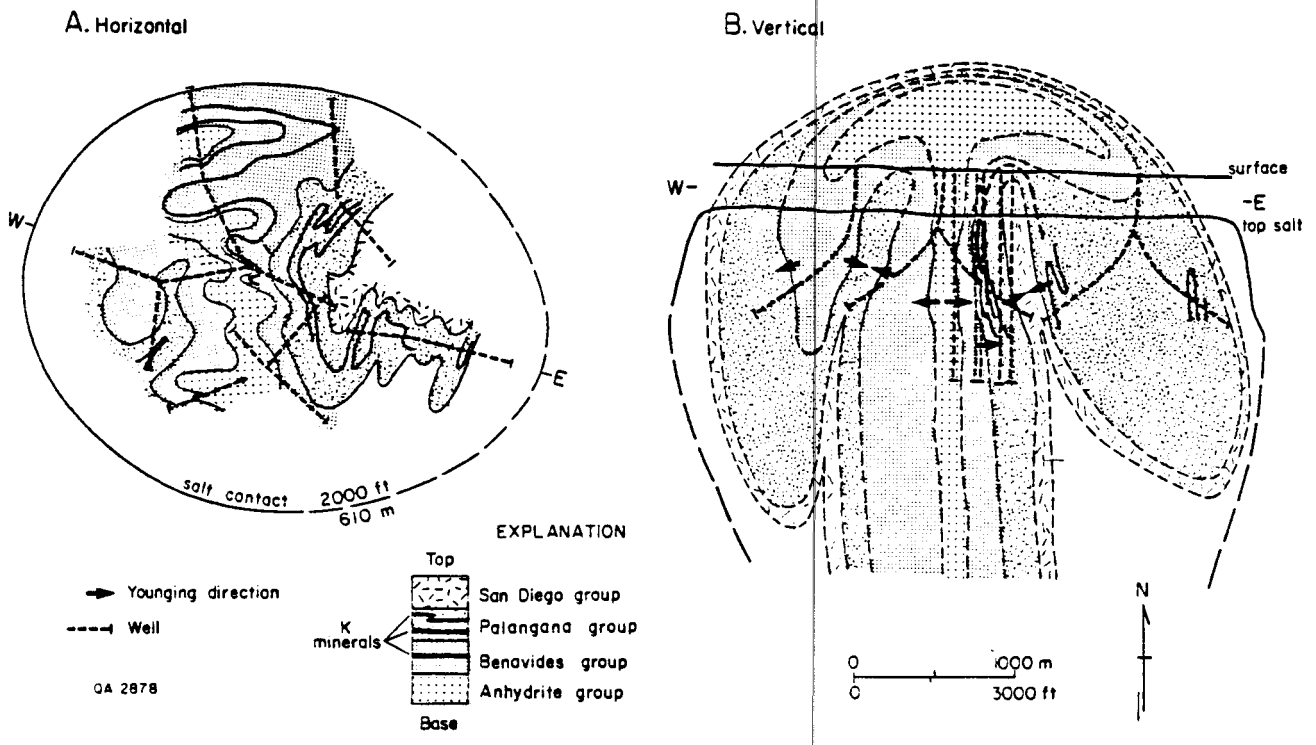


Figure 18. Palangana Dome, South Texas. H, horizontal section through dome at 610-m level, based on potash exploration using deviated wells (from Hofrichter, 1968). V, W-E vertical section through dome; solid lines from Hofrichter (1968); dashed lines show extrapolated structure interpreted as a fivefold mushroom diapir on the basis of stratigraphy and comparison with model domes. Stratigraphy: 1, Anhydritic group; 2, Benavides group (potash bearing); 3, Palangana group (potash bearing); 4, San Diego group. (After Talbot and Jackson, in preparation.)

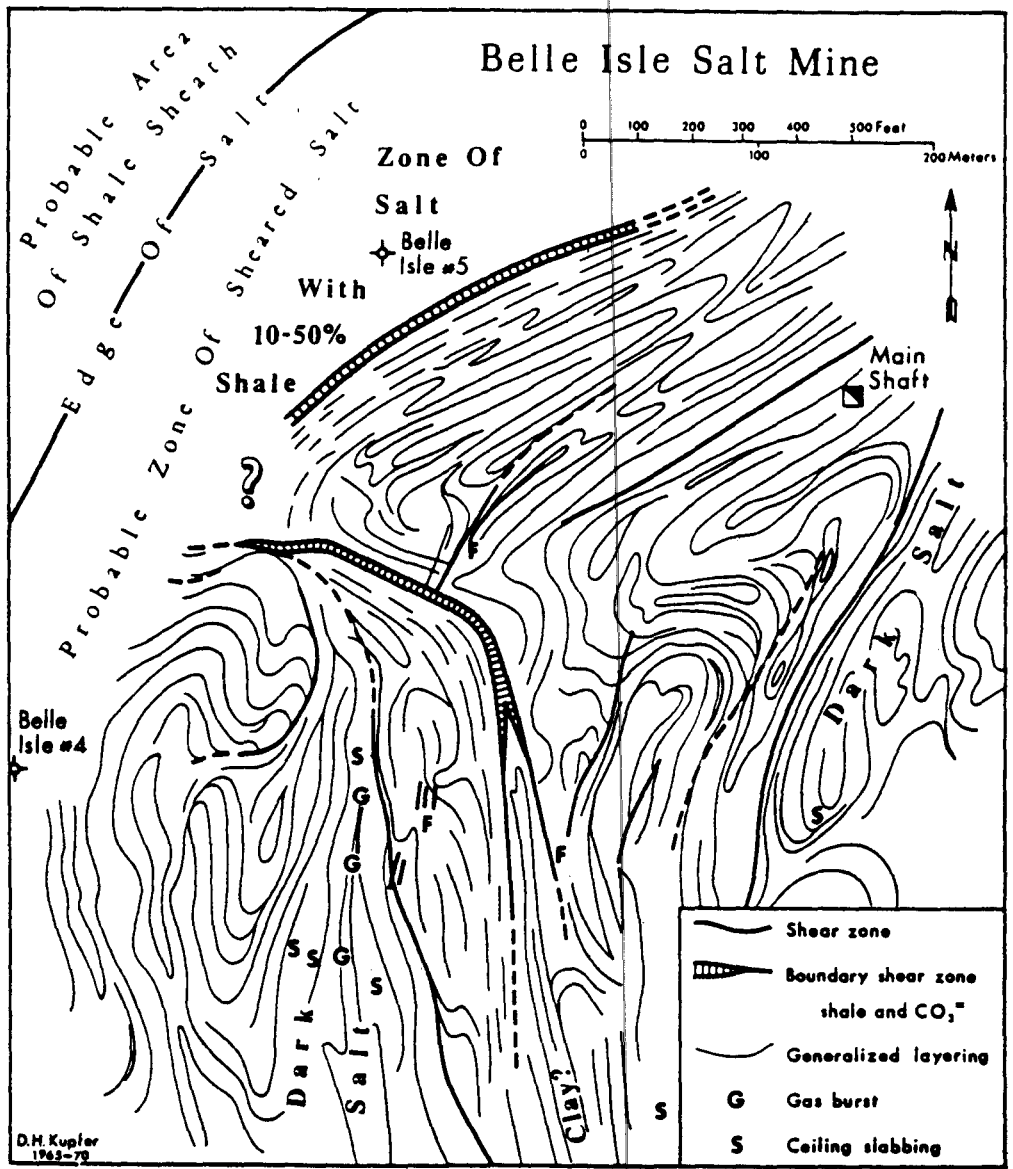


Figure 19. Horizontal section through northwest sector of Belle Isle Dome, Louisiana, at the mined 354-m level. The near-vertical boundary shear zone consists of halite with inclusions of shale and sandstone country rock. It may represent an infold of country rock into a mushroom-shaped salt diapir. (From Kupfer, 1974.)

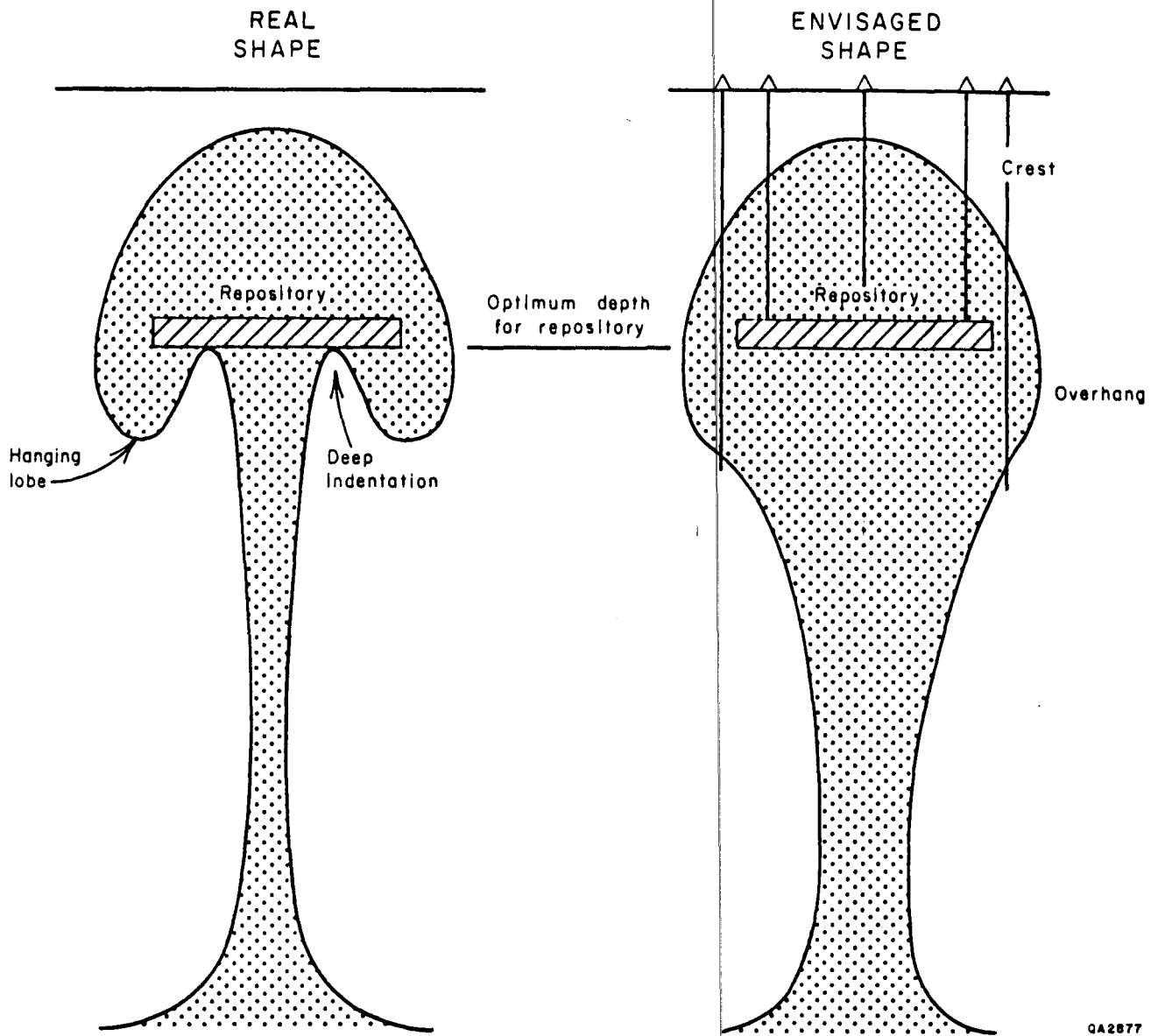
layer, has carried these Oligocene inclusions 7 km above the present level of the Oligocene strata flanking the stock. Kupfer (1974) believed that the included sediments were derived from above by trapping between two rising tongues of salt. However, on the basis of model evidence, it is at least as probable that the shale was trapped from below an overhang as an IAS infold. Belle Isle Dome is known to have an overhang on its northwest side (Murray, 1968), the side from which the shale-inclusion zone pierces the dome. Too little of the dome has been explored to prove or disprove this suggestion. But, regardless of its origin, the zone of shale inclusions represents an avenue of enhanced permeability possibly connecting the interior of the dome to the surrounding country rocks.

SOME IMPLICATIONS TO NUCLEAR WASTE ISOLATION

1. Mushroom-shaped diapirs are those with a peripheral hanging lobe surrounding an infold of country rock in the floor of the cap overhang. Such diapirs form experimentally wherever the effective viscosities of the diapiric material and its overburden are similar.

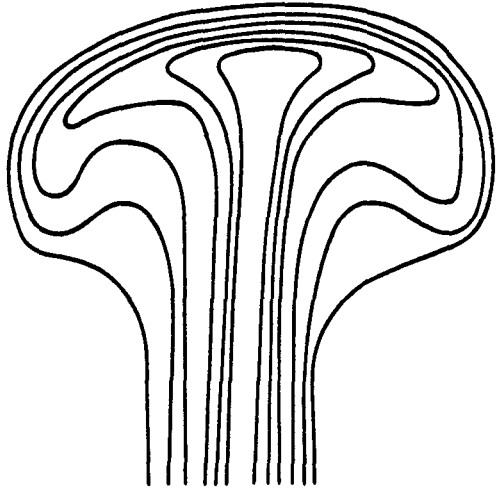
2. Current estimates of the effective viscosities of diapiric rock salt and its overburden indicate that mushroom diapirs or the type known as balloon on thread (types B and C, fig. 3) are probable in nature. Several natural salt diapirs in Canada, West Germany, and the U.S., including Palangana Dome in South Texas, resemble model mushroom diapirs and indicate that natural mushroom diapirs also exist.

3. The possibility of mushroom diapirs existing in nature has important implications for any repository built in a salt dome (fig. 20): the infold of country rock could reduce the "security zone" of rock salt below the repository. The degree of threat depends upon the size of the infold. If this is small and completely internal (figs. 10A and 21A), the infold consists entirely of salt and is not dangerous. If the infold is larger and involves the country rock as well (fig. 21B), the structure is potentially threatening; the closer the viscosities of salt and cover, the more likely this structure is to form. Infolded country rock may exist in Gorleben Dome in West Germany and has not been disproved by drilling (fig. 17). Permeable country

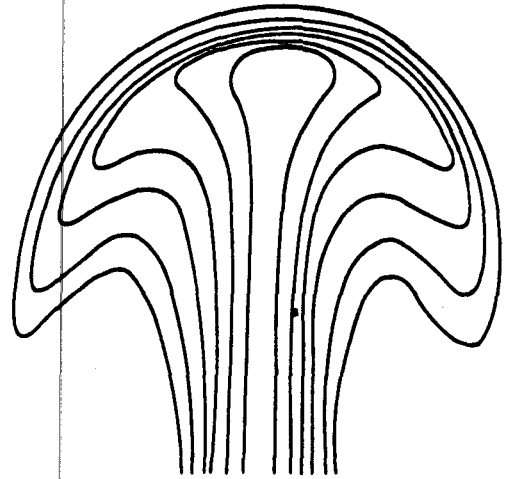


QA2877

Figure 20. The effect of salt dome shape (vertical sections) on the integrity of a repository. Left, a dome with hanging lobes (PSA) and deep indentations (IAS) into the base of the overhang threatening repository security. Dome shape after a dome modeled by the finite-element method (Berner and others, 1972). Right, a false shape of the dome envisaged only on the basis of subsurface exploration to the depth of the repository and through outer parts of the overhang.



A. Internal mushroom structure



B. External mushroom structure
QA2876

Figure 21. A. Internal mushroom structure has IAS infold and PSA downfold composed of evaporites entirely within diapir cap. B. External mushroom structure has IAS infold and PSA downfold composed of country rock and evaporites both outside and inside the dome.

rocks could allow ingress of water deep into the dome. For this reason, the part of Gorleben Dome intersected by cross section C-C' in figure 17 is safer than the part to the northeast because in the southwest the IAS infold is known to be cored by evaporites rather than by country rocks.

4. Another less common but equally dangerous structure is the double diapir structure, in which a thin zone of country rock is infolded between two diapirs that appear to be a single diapir from the outside (fig. 11). A zone of infolded country rock represents a built-in plumbing system of permeable rock capable of promoting fluid exchange between the heart of a double diapir and its surrounding overburden. Asse Dome in West Germany is a double diapir, but the critical infolded syncline consists of Zechstein evaporites rather than country rock.

5. To properly recognize and understand a mushroom structure to the point where its shape can be predicted during exploration, we need either (1) a good vertical section, obtainable from deep, closely spaced vertical drill holes or (2) a good horizontal section (as in a series of salt caverns or horizontal drill holes) combined with correlatable internal units. Way-up stratigraphic structures are extremely helpful, though not essential, for interpretation.

ACKNOWLEDGMENTS

This research was funded by the U.S. Department of Energy Office of Nuclear Waste Isolation under contract no. DE-AC97-83WM46651. Hans Ramberg, Ruud Weijermars, Peter Rönnlund, and Pierre Heeroma (University of Uppsala), kindly provided suggestions and comments on the experiments in Uppsala. Ronald Arvidsson (University of Uppsala) assisted greatly in material preparation and testing and model construction. Reinold Cornelius (Bureau of Economic Geology) prepared all the vertical and horizontal cross section diagrams of model domes and the block diagrams derived from these cross sections and also provided valuable suggestions. Figures were drawn by Jana Brod, Margaret L. Evans, Jamie A. McClelland, Nan Minchow-Newman, and Kerza A. Prewitt under the supervision of Richard L. Dillon. The text was word processed by Lisa L. Poppleton under the supervision of Lucille C. Harrell and edited by Amanda R. Masterson.

REFERENCES

- Berner, H., Ramberg, H., and Stephansson, O., 1972, Diapirism in theory and experiment: *Tectonophysics*, v. 15, p. 197-218.
- Bornemann, Otto, 1982, Stratigraphie und Tektonik des Zechsteins im Salzstock Gorleben auf Grund von Bohrerergebnissen: *Zeitschrift deutsche geologische Gesellschaft*, v. 133, p. 119-134.
- Carter, N. L., and Hansen, F. D., 1983, Creep of rocksalt: *Tectonophysics*, v. 92, p. 275-333.
- Dobrin, M. D., 1941, Some quantitative experiments on a fluid salt-dome model and their geological implications: *American Geophysical Union Transactions*, v. 22, pt. 2, p. 528-542.
- Essaid, Said, and Klarr, Konrad, 1982, Zum Innenbau der Salzstruktur Asse: *Zeitschrift deutsche geologische Gesellschaft*, v. 133, p. 135-154.
- Heard, H. C., 1972, Steady-state flow in polycrystalline halite at pressure of 2 kilobars, *in*, Heard, H. C., Borg, I. Y., Carter, N. L., and Raleigh, C. B., eds., *Flow and fracture of rocks*: Washington, D.C., American Geophysical Union, Geophysical Monograph Series Volume 16, p. 191-210.
- Heye, Dietrich, 1978, Experimente mit viskosen Flüssigkeiten zur Nachahmung von Salzstrukturen: *Geologische Jahrbuch*, v. E 12, no. 12, p. 31-51.
- _____ 1979, Modellversuche zum Salzdiapirismus mit viskosen Flüssigkeiten: *Geologische Jahrbuch*, v. E 16, p. 39-51.
- Hofrichter, Erich, 1968, Stratigraphy and structure of the Palangana salt dome, Duval County, Texas: *Geological Society of America Special Paper* 88, p. 365-379.
- Hunsche, Udo, 1978, Modellrechnungen zur Entstehung von Salzstockfamilien: *Geologische Jahrbuch*, v. E 12, p. 53-107.
- Jackson, M. P. A., 1984, Centrifuge modeling of the internal structure of mushroom-shaped diapirs: *Geological Society of America Abstracts with Programs*, v. 16, no. 6, p. 549.

- Jackson, M. P. A., and Talbot, C. J., in preparation, External shapes and dynamics of salt structures: submitted to Geological Society of America Bulletin.
- Kupfer, D. H., 1974, Boundary shear zones in salt stocks, in Coogan, A. H., ed., Fourth Symposium on Salt: Cleveland, Ohio, Northern Ohio Geological Society, v. 1, p. 215-225.
- LeCompte, P., 1965, Creep in rock salt: *Journal of Geology*, v. 73, p. 469-484.
- Murray, G. E., 1968, Salt structures of Gulf of Mexico Basin--a review, in Braunstein, J., and O'Brien, G. D., eds., Diapirism and diapirs: American Association of Petroleum Geologists Memoir 8, p. 99-121.
- Paine, W. R., Mitchell, M. W., Copeland, R. R., Jr., and Gimbrede, L. de A., 1965, Frio and Anahuac sediment inclusions, Belle Isle salt dome, St. Mary Parish, Louisiana: American Association of Petroleum Geologists Bulletin, v. 49, no. 5, p. 616-620.
- Ramberg, H., 1981, Gravity, deformation and the Earth's crust in theory, experiments and geological application, (2d ed.): London, Academic Press, 452 p.
- Schwerdtner, W. M., and Osadetz, Kirk, 1983, Evaporite diapirism in the Sverdrup Basin: new insights and unsolved problems: *Canadian Petroleum Geology Bulletin*, v. 31, no. 1, p. 27-36.
- Spiers, C. J., Urai, J. L., Peach, C. J., and Zwart, H. J., in press, The effect of brine (inherent and added) on rheology and deformation mechanisms in salt rock: Second Conference on Mechanical Properties of Salt, Hanover, extended abstract.
- Talbot, C. J., and Jackson, M. P. A., in preparation, Internal dynamics of salt diapirs.
- Tozer, E. T., and Thorsteinsson, R., 1964, Western Queen Elizabeth Islands, Arctic Archipelago: Geological Survey of Canada Memoir 332, 242 p.
- Tucker, P. M., and Yorston, H. J., 1973, Pitfalls in seismic interpretation: Society of Exploration Geophysicists Monograph Series No. 2, 50 p.
- Van Dyke, Milton, 1982, An album of fluid motion: Stanford, California, Parabolic Press, 176 p.
- Whitehead, J. A., Jr., and Luther, D. S., 1975, Dynamics of laboratory diapir and plume models: *Journal of Geophysical Research*, v. 80, no. 5, p. 705-717.

Woidt, W.-D., 1978, Finite element calculations applied to salt-dome analysis: Tectonophysics, v. 50, p. 369.

_____ 1980, Analytische und numerische Modellexperimente zur Physik der Salzstockbildung: Institut für Geophysik und Meteorologie der Technischen Universität Braunschweig GAMMA 38, 151 p.

**APPENDIX 1. SUMMARY OF EXPERIMENTS CARRIED OUT IN MARCH AND APRIL 1984,
AT THE HANS RAMBERG TECTONIC LABORATORY, UPPSALA, SWEDEN**

Experiment Number	Cover Loading Conditions	Dynamic Scaling	Maximum Accel. (g)	Cover Increments	Periods of Accel.	Internal Markers	Diapir Initiation	Description and Comments	Application
Note a	b	c	d	e	f	g	h		i
Aggrading Group									
022084	D, A	no	1,200	6	6	0	no	Carried out by CJT in February to evaluate technical feasibility of experimental downbuilding. Successful.	2
022184	U, A	no	1,200	1	8	0	no	Ditto to compare with downbuilding. Successful.	2
840307	D, A	rough	1,200	3	3	8	yes	First-order diapir overmatured, but second-order ones show best asymmetric internal structures.	1
840310	U, A	no	1,200	1	1	10	yes	To test effectiveness of upbulge versus downbulge in initiating domes. Successful.	1
840312-A	D, A	yes	1,200	5	5	16	no	"Salt, carbonate, dense shale, mixed shale and sandstone." Successful.	124
840312-B	U, A	yes	1,200	1	3	16	no	Same as 840312-A except for upbuilding. Successful.	124
840313	U, A	no	1,200	1	6	8	yes	Same as 840310 except initiators more widely spaced. Unsuccessful.	1
840314-A	U, A	no	1,200	1	5	0	no	Viscosity ratio $m=1$. Successful.	4

APPENDIX 1 (continued) Page 2 of 4

	840314-B	D, A	yes	1,200	5	5	16	no	Same as 840312-A except "carbonate" layer added in three increments and total cover thinner. Successful.	124
	840315	U, A	no	1,200	1	4	0	yes	Viscosity ratio $m < 1$. Successful.	4
	840316	U, A	no	1,200	1	10	0	no	Viscosity ratio $m > 1$. Unsuccessful.	4
	840319-A	D, A	yes	1,200	4	5	16	no	Same as 840314-B except "dense shale" replaces "carbonate." Successful.	124
	840319-B	U, A	yes	1,200	1	5	16	no	Same as 840319-A except for upbuilding. Successful.	124
	840321-B	D, A	yes	1,200	1	7	4	no	Viscosity ratio $m \approx 1$. Successful.	124
45	840409	D, A	yes	1,200	3	3	0	no	Wedge-shaped source. Successful.	24
	840417	D, A	yes	1,200	5	5	9	no	Stepped source. Partly successful.	124
	840418	U, A	yes	1,200	1	5	9	no	Same as 840417 except for upbuilding. Partly successful.	124
	Prograding Group									
	840321-A	D, P	yes	1,200	4	4	8	no	Tabular layers of cover. Successful.	134
	840322	D, P	yes	1,200	4	4	4	no	Same as 840321-A except thinner source and cover to reduce wavelength. Successful.	134

APPENDIX 1 (continued) Page 3 of 4

46

840328	D, P	yes	1,900	5	5	4	no	Same as 840322 except stiffer and thinner source and cover. Successful.	134
840402	U, static half load	yes	1	1	1	4	no	Extreme differential loading. Successful.	134
840403	D, P	yes	1,900	5	5	4	no	Extreme lateral intrusion of diapir like Sigsbee Scarp. Successful.	134
840412	D, P	yes	890	18	18	8	no	Prograding rectangular, narrow prisms. Overmature.	134
840413	D, P	yes	1,200	20	20	7	no	Prograding triangular, narrow prisms. Successful.	134
840423	D, P	yes	1,200	4	5	8	no	Same as 840403 except stiffer cover. Successful.	134
Mercury Cover Group									
840410	U	no	1	1	1	0	no	Hg as thin, dense cover on rectangular source. Successful.	24
840411	U	no	1	1	1	0	no	Same as 840410 except circular source. Successful.	24
Piedmont Glacier Group									
P-1	-	no	450	0	6	49	-	Passive moraine layers, episodic flow. Successful.	1
P-2	-	no	530	0	11	38	-	Same as P-1, but softer "ice."	1

APPENDIX 1 (continued) Page 4 of 4

P-3	-	no	530	0	1+4	38	-	Same as P-2 except continuous flow followed by two surges. Successful.	1
P-4	-	no	450	0	5+1	70	-	Same as P-2 except flow over frictionless Hg, followed by surge. Successful.	1
P-5	-	no	1,900	0	8	23	-	Same as P-1. Successful until piedmont severed accidentally.	1
P-6	-	no	1,900	0	2	46	-	Passive and one active moraine layers, two surges over sideways tilted plain. Successful.	1
P-7	-	no	1,200	0	11+2	42	-	Passive and two active moraine layers, episodic flow plus two surges down rounded valley. Successful.	1

47

Notes

- a. Based on date that model preparation began; piedmont group experiments were carried out mainly in April, apart from P-1 in February by CJT.
- b. D, downbuilding diapirs; U, upbuilding diapirs; A, aggrading cover; P, prograding cover.
- c. Some models not purposely scaled may prove dynamically scaled by accident.
- d. Maximum acceleration calculated on basis of instrumented rpm for a datum level 10 mm above model floor.
- e. Number of times layers of cover were added before an acceleration.
- f. Number of periods of acceleration and deceleration of model.
- g. Number of marker layers in source layer (required for study of internal structure).
- h. Diapirs can be artificially localized by small bulges in upper surface of source layer acting as seeds.
- i. (1) Internal structures of diapirs; (2) downbuilding versus upbuilding structures; (3) prograding cover and differential loading; (4) large-scale movement cells in diapiric systems.

APPENDIX 2: EXPERIMENTAL PROCEDURE

The c.g.s. units quoted here can be converted to SI using the following conversion factors:

<u>To Convert From</u>	<u>To</u>	<u>Multiply By</u>
$\text{g}\cdot\text{cm}^{-3}$	$\text{kg}\cdot\text{m}^{-3}$	1,000
$\text{dyn}\cdot\text{cm}^{-2}$	$\text{Pa} = \text{N}\cdot\text{m}^{-2}$	0.1000
poise = $\text{dyn}\cdot\text{s}\cdot\text{cm}^{-2}$	$\text{Pa}\cdot\text{s} = \text{N}\cdot\text{s}\cdot\text{m}^{-2}$	0.1000

1.0 Model Materials

1.1 The following abbreviations are used, and dimensions are quoted in centimeter-gram-second units:

ρ = density ($\text{g}\cdot\text{cm}^{-3}$)

μ = effective dynamic viscosity (poise = $\text{dyn}\cdot\text{s}\cdot\text{cm}^{-2}$)

$\dot{\epsilon}$ = longitudinal strain rate (s^{-1})

$\dot{\gamma}$ = shear strain rate (s^{-1})

n = exponent of the power creep law relating strain rate, $\dot{\epsilon}$, (or shear-strain rate $\dot{\gamma}$) to normal stress, σ , (or shear stress τ) and a general coefficient C (a function of pressure, temperature, and other factors). In its simplest form the law is:

$$\dot{\epsilon} = C\sigma^n \quad [1]$$

$$\text{or } \dot{\gamma} = C\tau^n \quad [2]$$

In true (Newtonian) viscous fluids, $n = 1$, and the relationship is linear. For $n > 1$, the viscosity decreases with increasing stress or strain rate.

1.2 The principal materials and material mixtures used are listed on the next page, together with some of their rheologic properties.

Rhodorsil Gomme (RG), supplied by Rhône-Poulenc, Paris.

Batch 1: $\rho = 1.16 \text{ g}\cdot\text{cm}^{-3}$, $n = 1.0$, yield strength zero,

$$\mu = 3 \cdot 10^5 \text{ P at } \dot{\gamma} = 0.002\text{-}0.01 \text{ s}^{-1}$$

Batch 2: $\rho = 1.09 \text{ g}\cdot\text{cm}^{-3}$, $n = 1.2$, yield strength \approx zero to $3 \cdot 10^2 \text{ dyn}\cdot\text{cm}^{-2}$,

$$\mu = 3 \cdot 10^5 \text{ P at } \dot{\gamma} = 0.005\text{-}0.01 \text{ s}^{-1}$$

(Batch 2 was a new drum opened after the first drum, Batch 1, was exhausted.)

This is the basic pink silicone putty, an artificial visco-elastic mixture of silicone and powdered solids. It was used pure or mixed.

- 1.3 Plastilina is Swedish-made modeling clay (MC) equivalent to the better known British Plasticine, a mixture of oils, waxes, dyes, and mineral filler. Red MC was used where possible to standardize rheologic properties. It was used in pure form as a nonflowing, stiff floor or wall for the models and in mixtures with RG to stiffen the latter. The properties of Plasticine have been published as follows (McClay, 1976).

$$n = 6 \text{ to } 9, \mu = 3 \cdot 10^9 \text{ P at } \dot{\epsilon} = 1 \cdot 10^{-3} \text{ s}^{-1}, \mu = 5 \cdot 10^{11} \text{ P at } \dot{\epsilon} = 1 \cdot 10^{-6} \text{ s}^{-1}$$

- 1.4 75 RG/25 MC is a mixture of 75 wt. % RG (Batch 2) and 25 wt. % MC for moderately stiff mixtures.

$$\rho = 1.17 \text{ g}\cdot\text{cm}^{-3}, n = 1.2, \text{ yield strength} = 3 \cdot 10^2 \text{ dyn}\cdot\text{cm}^{-2}, \mu = 3 \cdot 10^5 \text{ P at } \dot{\gamma} = 0.003\text{-}0.01 \text{ s}^{-1}$$

- 1.5 50 RG/50 MC is a mixture of 50 wt. % RG (Batch 2) and 50 wt. % MC.

$$\rho = 1.26 \text{ g}\cdot\text{cm}^{-3}, n = 3.5, \text{ yield strength} = 10^4 \text{ dyn}\cdot\text{cm}^{-2}, \mu = 4 \cdot 10^5 \text{ P at } \dot{\gamma} = 0.002\text{-}0.01 \text{ s}^{-1}, \mu = 2 \cdot 10^5 \text{ P at } \dot{\gamma} = 0.02\text{-}0.04 \text{ s}^{-1}$$

- 1.6 50 RG/50 MC + 9.3% BaSO₄ is a mixture of 45.35 wt. % RG (Batch 2), 45.35 wt. % MC, and 9.30 wt. % BaSO₄ for increased density.

$$\rho = 1.34 \text{ g}\cdot\text{cm}^{-3}, n = 2.7, \text{ yield strength} = 8 \cdot 10^3 \text{ dyn}\cdot\text{cm}^{-2}, \mu = 9 \cdot 10^5 \text{ P at } \dot{\gamma} = 0.002\text{-}0.03 \text{ s}^{-1}$$

- 1.7 Mercury

$$\rho = 13.55 \text{ g}\cdot\text{cm}^{-3}, n = 1.0, \text{ yield strength zero}, \mu \approx 2 \cdot 10^{-2} \text{ P at any } \dot{\gamma}$$

2.0 Material Preparation

Layers were differentiated in models by mixing in powdered poster pigments, regardless of whether they were designed to differ in mechanical properties.

Density was increased by adding powdered barite (BaSO_4) or magnetite ($(\text{Fe}^{2+}\text{Fe}^{3+})_2\text{O}_4$). As a guide to proportions the following formula was used.

$$m_2 = \frac{m_1(\rho_1 - \rho_3)\rho_2}{\rho_1(\rho_3 - \rho_2)} \quad [3]$$

where m_2 = mass of additive, m_1 = mass of starter, ρ_1 = density of starter, ρ_2 = density of additive, and ρ_3 = density required. All densities were repeatedly checked. Proportions of constituents were weighed on a chemical beam balance to three significant figures.

Yield strength was increased by adding MC to RG. Increase in yield strength preserves model sections after they were cut. This also increases the n value, thus making the model material similar to real rocks. All mixing was done by hand kneading for approximately 20 minutes. For most experiments, bubbles induced by mixing were undesirable, so were largely expelled by centrifuging, after which the material was allowed to relax before model construction.

3.0 Material Testing

3.1 Density

Density of a 20-mm sphere of model material was determined by Archimedes's Principle on a chemical beam balance: volume was determined by measuring the apparent loss of mass when the previously weighed sphere was immersed in water; the sphere displaced a volume of water equal to its own volume and its mass was apparently diminished by the mass of water displaced.

$$\rho = \frac{m_a}{m_a - m_w} \quad [4]$$

where m_a = mass of sphere in air, m_w = mass of sphere in water.

Densities were measured to four significant figures and the procedure repeated. Each mass was corrected by subtracting the mass of the sphere's suspension cage (disk and wires) in air (2.080 g) and water (1.460 g). Bubbles within the model material were removed by centrifuging; bubbles clinging to the suspension cage were removed by agitation.

3.2 Effective Dynamic Viscosity

Viscosity was measured in a coaxial viscometer using cylindrical Couette flow. The apparatus was designed and built specifically for this purpose by technical staff in the Institute of Geology, Uppsala. Vertical coaxial cylinders were separated by the test material, which rested on

frictionless mercury. The inner cylinder rotated against the resistance of the viscous material under torque supplied by a known and variable mass. The outer cylinder was clamped stationary.

The following equations describe the relations between variables used to determine viscosity and n values.

$$\omega' = \frac{\alpha}{t} \quad [5]$$

$$\omega = \frac{\pi\omega'}{180} \quad [6]$$

$$\dot{\gamma} = C\tau^n \quad [2]$$

$$\tau = \frac{(m-m')g R}{2\pi r_i^2 h} \quad [7]$$

$$\dot{\gamma} = \frac{2n\pi\omega}{\left[1 - \left(\frac{r_i}{r_o}\right)^{2n}\right]} 180 \quad [8]$$

$$\mu = \frac{\tau}{\dot{\gamma}} \quad [9]$$

- where
- ω' = angular velocity of inner cylinder rotor (degrees s⁻¹)
 - ω = angular velocity of inner cylinder rotor (radians s⁻¹)
 - α = angle of rotation (degrees) during time t
 - $\dot{\gamma}$ = shear-strain rate along inner cylinder mantle (s⁻¹)
 - C = material constant
 - n = exponent in power-law creep: values of n > 1 are characteristic of non-Newtonian fluids, where strain rate is not linearly related to stress, but is proportional to a power n of the stress
 - π = 3.142
 - τ = shear stress along inner cylinder mantle (dyn·cm⁻²)
 - m = mass of weight applying moment of force (g)
 - m' = mass required to overcome apparatus friction (g)
 - g = 980.7 cm·s⁻² = standard value for acceleration due to gravity (free fall)
 - R = radius of rotor of inner cylinder (cm)
 - r_i = radius of inner cylinder (cm)
 - r_o = radius of outer cylinder (cm)
 - h = height of annulus of test material between cylinders (cm)

The test procedure was as follows:

3.2.1 Test materials were homogenized by mixing and loaded into the viscometer to avoid any preferred orientation. Air trapped during loading was driven out in a centrifuge, after which the material was allowed to relax for at least 12 h before testing. Measurements were carried out at $\sim 21^\circ\text{C}$ at low strain rates ($\dot{\gamma} \approx 10^{-2} \text{ s}^{-1}$) comparable to those during centrifuge acceleration. From four to nine different masses ($m-m'$) were applied to each test material. α was plotted against t in 10 increments (measured by an electronic digital stopwatch with lap functions). ω' was calculated by equation 5 and converted to ω using equation 6.

3.2.2 For each test material a single graph of $[\log \omega']$ versus $\left[\log \left(\frac{m-m'}{h} \right) \right]$ was prepared. The slope of this line is equivalent to the n value of power-law creep, which is related to shear stress and strain rate by the general equation 2.

3.2.3 For each test material a single graph of τ versus $\dot{\gamma}$ was prepared. τ was calculated by equation 7, and $\dot{\gamma}$ was calculated by equation 8. The material viscosity was calculated using the slope of the curve on this graph according to equation 9. For non-Newtonian materials ($n \neq 1$), the slope of this curve (hence viscosity) varies with shear-strain rate.

4.0 Model Design

Many aspects of model design are artistic and creative rather than technical and mechanical. Such aspects cannot be formally documented. An exception is the technical procedure of scaling. Scaling is the formal relation between a model and its prototype in nature, as expressed in model ratios of length, density, viscosity, strength, body force, stress, strain, and time. Geometric scaling applies if the model is a smaller geometric replica of the original. Kinematic scaling applies if the model imitates the movements and velocities of the original at a scale corresponding to its reduced size. Dynamic scaling applies if the ratio is constant between the different mechanical forces (gravity, inertia, viscous, elastic, frictional, and stress forces) in the original and in a geometrically and kinematically scaled model. The theory and practice of scaling are complex. Procedures followed those documented in Hubbert (1937) and Ramberg (1981), both of which were based on engineering practices.

Most models were scaled. Dynamic scaling is desirable if a model is intended to be an analogue of and guide to real salt domes. Dynamic scaling is

not necessary if the model is intended merely as a demonstration of general principles.

4.1 Model Construction

Models were constructed using simple tools (cutters, rollers, templates, rulers, and vernier calipers) that had evolved over 20 years of use in this laboratory. Stacked sheets of material formed the basis for most models. Sheets were made by rolling, initially using a heavy solid steel roller, followed by a light tubular aluminum roller. Constant or tapering thicknesses were produced by resting the ends of the roller on machined plastic strips and wedges of various standard thicknesses (in mm).

Disks (or portions of disks) were cut out of the sheets using 10-cm template rings or a sharp knife and stacked to build a model. Downbuilding models had successive layers added between accelerations in the centrifuge. Upbuilding models were completely built before centrifuging. The base, and in some models, the walls, of the model were built out of stiff MC. The outer surface of the base and walls was then lined with polythene to prevent sticking and placed in an aluminum centrifuge cup 10 cm in diameter and 5 to 8 cm high. Between the model and the cup floor was placed a machined plastic equipotential disk, 10 cm in diameter, with a planar lower surface and a cylindrically concave upper surface angled so the axis of the concavity was lower on one side than on the other side; the unique lowest part of the disk was aligned with an arrow (the equipotential arrow) imprinted on the model with marker pen or lead pencil. This disk gently deformed the model so that the horizontal layers in the model were parallel to the equipotential surface in the centrifuge during acceleration. The form of the equipotential surface (a surface of equal acceleration) is roughly that of the walls of a vertical cylinder and varies slightly with the angular velocity of the cup during acceleration. For this reason most experiments were run at a standard velocity.

A millimeter-scale grid could be printed in the upper surface of the model using photocopies of graph paper produced by an offset printing technique. This grid enabled the surface strains to be monitored during centrifuging and subsequently mapped from photographs.

5.0 Model Acceleration

A few experiments were run at normal gravity of 1 g. Acceleration began as soon as the dense overburden was applied. Extreme instability was induced by

the addition of mercury overburden. The resulting gravitational overturn took place within 2 hours. Such experiments were run on the photographic bench (see next section) for documentation.

Most of the experiments were run with high artificial accelerations in the medium-capacity centrifuge. The accelerations in terms of g were determined from instrumented rpm using a nomogram prepared by Professor Hans Ramberg. Graphs showing the acceleration for models of different heights were prepared from the nomogram. Equations relating centrifugal force (F_c) and centrifugal acceleration (a_c) are:

$$F_c = mr\omega^2 \quad [10]$$

where a body of mass m describes a circular path of radius r at an angular velocity ω ($\text{rad}\cdot\text{s}^{-1}$).

$$a_c = r\omega^2 \text{ (cm}\cdot\text{s}^{-2}\text{)} \quad [1]$$

$$a_c = \frac{r\omega^2}{980.7} \text{ (units of } g\text{)} \quad [2]$$

The model and enclosing cup were counterweighted by an equal mass in the opposite container of the centrifuge rotor. The model and its cup were loaded so that the equipotential arrow on the model was aligned toward the rotor axis. A small disk on the rotor axis was aligned to a pre-marked direction to synchronize the stroboscopic light so that the model could be clearly seen while spinning. The lid of the centrifuge housing was closed after checking that the strobe indicator light was on. The spinning speed (angular velocity) of the centrifuge rotor was altered by a gear system with continuous gear ratios up to maximum speed (3,000 rpm). For any gear setting, the speed gradually increased to a maximum. Each run, or step, comprised periods of accelerating, constant, and decelerating speeds, which were timed with a stopwatch. Care was taken to accelerate the rpm as rapidly as possible to the required speed by manipulation of the gear system; rapid deceleration was possible by applying a hand brake after switching off the motor. The spinning time was either predetermined or decided during the experiment on the basis of viewing the model in stroboscopic light through an observation port. Strong fans blew chilled air from refrigerated coils onto the model to cool it during runs lasting more than 2 minutes.

6.0 Model Dissection and Documentation

Each model was chilled in a small freezer in the laboratory before cutting to prevent model materials deforming during cutting. Cutting by hand requires

great skill because of the rheology of RG compounds; no mechanical devices have been found to be of practical use. Each slice was cut 2 to 3 mm thick by rapid, light strokes along an aluminum straightedge using a scalpel with a sharp blade 5 to 10 cm long dipped in cold water between strokes. Single slices were taken between some centrifuge runs to document successive growth stages; these were labeled as step 1, 2, etc. On completion of centrifuging, the entire model was generally cut in two and each half sectioned into horizontal and vertical slices, respectively; these were labeled as serial sections. Some models were only sectioned vertically.

Each slice was labeled and photographed in groups arranged in sequence on a background of mm graph paper for scale. Photography was on a copy stand with four floodlights using a Nikkormat camera and macrolens loaded with Kodachrome 64 daylight positive film and mounted on a heavy camera stand. Typically, photographs were taken in triplicate, one copy remaining in Uppsala. Models were numbered with a six-digit number according to the SI date on which model construction began (e.g., 840307). A letter suffix differentiates models that began to be built on the same day.

After photography, slices were frozen and stored in drawers in a cold room in the Institute of Geology set aside specifically for this purpose. Subsequent survival of the model depended entirely on the materials used. Those made out of RG have virtually no yield strength and they distorted by flow after several weeks even in cold temperatures. Those made out of 75 RG/25 MC or 50 RG/50 MC have a sufficiently high yield point to survive intact. A few models were brought back to Austin as examples, but despite careful packing some of these were distorted by flow. They are stored in room 2.102M at the Bureau of Economic Geology. As described in the next section, all analysis is done on the macroscopic photographic images (rather than the actual models), which record the pristine state of all model slices.

References

- Hubbert, M. K., 1937, Theory of scale models as applied to the study of geologic structures: Geological Society of America Bulletin, v. 48, p. 1459-1520.
- McClay, K. R., 1976, The rheology of Plasticine: Tectonophysics, v. 33, p. T7-T15.
- Ramberg, Hans, 1981, Gravity, deformation and the Earth's crust, Second Edition: London, Academic Press, 452 p.

APPENDIX 3: ANALYTICAL PROCEDURE

1.0 Introduction

This section provides instructions for analyzing and synthesizing data obtained from experimental modeling of salt diapirs by centrifuging, as described in Appendix 2. The data are in the form of color slides of slices of models, obtained by methods outlined in Appendix 2.

2.0 Data Handling

All color slides were catalogued and each slide mount labeled with a unique number, the number of the experiment that yielded the slice(s) photographed, and information on the orientation of the slice. One complete set is used exclusively for working with. A less complete duplicate set is stored in a separate file as a backup set for security purposes.

Half-model (semicircular) horizontal plane sections are numbered from bottom to top (arabic numerals). Layers in the model are individually numbered (in the source multilayer) or lettered (in the cover multilayer) from bottom to top in stratigraphic order.

Vertical sections are numbered from the inside to the outside of the model. Near and far refer to the directions of the model axis and model walls, respectively. Individual domes in vertical sections are numbered from left to right in roman numerals.

3.0 Analysis and Synthesis

Color slides are projected on paper pinned to a wall, yielding an image enlarged to a scale large enough to show all the details of the visible deformation. Typical enlargements are between 2.5 and 7.5 times the original model size.

Different types of drawings were made for different purposes. For example, layers within the source multilayer were mapped for the study of internal (within dome) structures. These internal layers were omitted for study of the relation between dome shape and cover. Examples of these diagrams are:

- 1) Plan section, source top

- 2) Plan section, source top and cover layers
- 3) Plan section, domes with internal marker layers
- 4) Vertical section, source top
- 5) Vertical section, source top and cover layers
- 6) Vertical section, domes with internal marker layers

Serial vertical sections of models were graphically combined into parallel fences to demonstrate three-dimensional relations. Structure contour maps on top of the source layer were constructed from these parallel fences by directly reading elevations in sections, posting these on a map, and contouring posted values.

Serial horizontal sections of models were used to simulate the mine maps in salt domes at different levels. These sections were also used to construct block diagrams in isometric projection, using one contact in each horizontal section as a structure contour on that contact. One structure contour from each section was combined with that from other sections to produce a structure-contour map analogous to that produced from serial vertical sections. This was then digitized and skewed by programs SKEW2 (number GR0070.00.00) and BDIG12 (number GR0080.00.00). The resulting skewed contours were then incrementally translated (using the technique described by Lobeck, 1924) by a vertical distance z equal to the mean thickness of each slice:

$$z = \frac{h_m}{n} \quad [14]$$

where h_m is the height of the model

n is the number of horizontal slices in the model

Reference

Lobeck, A. K., 1924, Block diagrams and other methods used in geology and geography: New York, John Wiley, 186 p.